Repository of the Max Delbrück Center for Molecular Medicine (MDC) in the Helmholtz Association

http://edoc.mdc-berlin.de/15874

Amyloid-{beta}(1-42) aggregation initiates its cellular uptake and cytotoxicity

Jin, S. and Kedia, N. and Illes-Toth, E. and Haralampiev, I. and Prisner, S. and Herrmann, A. and Wanker, E.E. and Bieschke, J.

Amyloid-β(1–42) Aggregation Initiates Its Cellular Uptake and Cytotoxicity*[S]

Sha Jin[‡§], Niraja Kedia[§], Eva Illes-Toth[§], Ivan Haralampiev[¶], Simon Prisner[¶], Andreas Herrmann[‖], Erich E. Wanker[‡], and Jan Bieschke[§1]

From the [‡]Proteomics and Molecular Mechanisms of Neurodegenerative Diseases, Max Delbrück Center for Molecular Medicine, 13125 Berlin–Buch, Germany, the [§]Department of Biomedical Engineering, Washington University, St. Louis, Missouri 63130, the [¶]Department of Biology and [‖]IRI Life Sciences, Humboldt–Universität zu Berlin, 10115 Berlin, Germany

The accumulation of amyloid β peptide(1–42) (Aβ(1–42)) in extracellular plaques is one of the pathological hallmarks of Alzheimer disease (AD). Several studies have suggested that cellular reuptake of Aβ(1–42) may be a crucial step in its cytotoxicity, but the uptake mechanism is not yet understood. Aβ may be present in an aggregated form prior to cellular uptake. Alternatively, monomeric peptide may enter the endocytic pathway and conditions in the endocytic compartments may induce the aggregation process. Our study aims to answer the question whether aggregate formation is a prerequisite or a consequence of Aβ endocytosis. We visualized aggregate formation of fluorescently labeled Aβ(1–42) and tracked its internalization by human neuroblastoma cells and neurons. β-Sheet-rich Aβ(1–42) aggregates entered the cells at low nanomolar concentration of Aβ(1–42). In contrast, monomer uptake faced a concentration threshold and occurred only at concentrations and time scales that allowed Aβ(1–42) aggregates to form. By uncoupling membrane binding from internalization, we found that Aβ(1–42) monomers bound rapidly to the plasma membrane and formed aggregates there. These structures were subsequently taken up and accumulated in endocytic vesicles. This process correlated with metabolic inhibition. Our data therefore imply that the formation of β-sheet-rich aggregates is a prerequisite for Aβ(1–42) uptake and cytotoxicity.

One of the pathological hallmarks of Alzheimer disease (AD)[2] is the presence of extracellular plaques composed mainly of 42-amino acid amyloid β peptide (Aβ(1–42)) (1). The small hydrophobic Aβ(1–42) peptide, which is generated by proteolytic cleavage of the amyloid precursor protein, is released as a monomer from the plasma membrane into extracellular space, and tends to aggregate spontaneously into oligomeric, protofibrillar, and fibrillar assemblies (2–4). Oligomeric species of Aβ(1–42) are tightly linked to AD pathogenesis and are presumed to be the cause of neuronal damage (5). Several studies have suggested that the reuptake of extracellular Aβ(1–42) into neurons may lead to the formation of intracellular aggregates, resulting in neuronal damage and neurotoxicity (6–8). Endocytosis of misfolded proteins has also been observed in cell models of the tau protein, α-synuclein and huntingtin (9, 10), and recent evidence suggests that it may be the initial step in the replication of the misfolded protein structures by prion mechanisms (10–14). Several possible endocytic pathways, such as macropinocytosis and receptor-mediated endocytosis, have been discussed for Aβ and other misfolded protein aggregates (15–19). However, our understanding of the connection between aggregation and cytotoxicity is still limited. It has not been conclusively determined how and when the Aβ(1–42) peptide becomes toxic, whether Aβ aggregates prior to internalization or during the internalization process and, if so, in which intracellular compartments the aggregates form. Elucidating the connection between aggregation and internalization of Aβ(1–42) peptide may be thus vital in understanding its toxicity.

Here, we examine the relationship between the aggregation state of extracellular Aβ(1–42) and the efficiency of its internalization. We aimed to determine whether the formation of aggregates and particularly β-sheet-rich structures, as reported by thioflavin dyes (20) and conformation-specific antibodies is a prerequisite for its neuronal uptake.

We found that cultured human neuroblastoma cells (SH-EP cells) can efficiently internalize β-sheet-rich aggregates of Aβ(1–42) at nanomolar concentrations, and that cellular uptake was associated with metabolic inhibition. In contrast, monomeric Aβ(1–42) only entered cells inefficiently and at high nanomolar concentrations. Internalization occurred after aggregation on the plasma membrane, which suggests that the membrane is an environment that facilitates aggregation of Aβ(1–42) monomers.

Results

Preparation and Characterization of Fluorescently Labeled Aβ(1–42)—To investigate the relationship between the aggregation state of Aβ(1–42), its internalization and cytotoxicity,

[S] This article contains supplemental Fig. S1.

[1] To whom correspondence should be addressed. Tel.: 314-935-7038; E-mail: bieschke@wustl.edu.

[2] The abbreviations used are: AD, Alzheimer disease; Aβ(1–42), amyloid β peptide-(1–42); AFM, atomic force microscopy; CME, clathrin-mediated endocytosis; HCS, high-content screening; IF, immunofluorescence staining; MTT, 3-(4,5-dimethylthiazol-2-yl)-2,5-diphenyltetrazolium bromide; SEC, size exclusion chromatography; ThT, thioflavin T; ThS, thioflavin S; Tf, transferrin.

we examined whether the presence of the secondary structure determines the behavior of Aβ(1–42) toward the cells and membranes. Aggregated Aβ, which may contain oligomers, protofibrils, and fibrils, was classified in two populations: a state without β-sheet structure and a state in which β-sheets have been formed. Concentrations of aggregated Aβ(1–42) peptide are expressed in terms of their amount of Aβ monomers as "equivalent monomer concentration."

To track the peptide and to observe aggregation of monomeric Aβ(1–42) in cultured cells, we generated Aβ(1–42) peptides that were fluorescently labeled at the N terminus with Atto565-maleimide (Aβ(1–42)[565]), Atto488-maleimide (Aβ(1–42)[488]), or Atto633-maleimide (Aβ(1–42)[633]) as described below. Labeled Aβ(1–42) was separated by size exclusion chromatography (SEC, Fig. 1A). Aβ eluted in two populations at 0.86 (protofibrils, PF) and 1.39 ml (monomer, M).

We used unlabeled monomers and aggregation-incompetent sc-Aβ(1–42)[565] as controls on SEC, both of which eluted similar to the Aβ(1–42)[565] monomer fraction (M, Fig. 1A). Those monomers could not be detected by atomic force microscopy (AFM, Fig. 1B). In contrast, AFM identified the PF fraction of Aβ(1–42)[565] to be protofibrils with an average height of 4 nm (Fig. 1B). When incubated with ThT, the protofibrils (35 μM monomer equivalent) bound the dye immediately and ThT fluorescence changed little over the course of 1 h, whereas ThT fluorescence of the monomeric Aβ (35 μM) displayed sigmoid kinetics typical of nucleated polymerization (Fig. 1C).

To further examine whether the fluorescence label influenced Aβ(1–42) monomer aggregation, we compared fibril formation kinetics and fibril morphologies of labeled and unlabeled Aβ(1–42). Unlabeled monomeric Aβ(1–42) was mixed with 10% Aβ(1–42)[565] (total Aβ(1–42) concentration of 15 μM) and incubated in PBS at 25 °C. Aggregation kinetics were monitored by binding of ThT *in vitro* (Fig. 1D) (21). The addition of 10% Aβ(1–42)[565] monomer slowed the formation of fibers only slightly, without changing fibril structure, as observed by AFM (Fig. 1, D and E). We imaged fibrils formed in the presence of Aβ(1–42)[633] by fluorescence microscopy using ThT fluorescence and Aβ(1–42)[633] fluorescence (Fig. 1F). A high degree of correlation between the signals in both channels demonstrated that all fibrils did indeed incorporate labeled Aβ(1–42) (Fig. 1G).

We used labeled monomers (M) and protofibrils (PF, Fig. 1B) to compare their respective cellular uptake. Mature fibrils (Fig. 1E) were used to compare their uptake to that of protofibrils and monomers. For kinetic analysis of cellular uptake mixtures of 90% unlabeled Aβ(1–42) and 10% Aβ(1–42)[565] were used.

Efficient Uptake of Aβ(1–42) Protofibrils—We treated cultured human neuroblastoma (SH-EP) cells with Aβ(1–42)[565] monomers or protofibrils to determine whether both Aβ species are internalized differently. Cells were imaged by confocal microscopy after incubation with Aβ(1–42)[565] at 37 °C for 24 h (Fig. 2, A–E). A soluble membrane-impermeable fluorescent dye, calcein (20 μM), was added to the extracellular medium to mark the uptake of extracellular medium during vesicular trafficking from the plasma membrane into the cells in endocytic vesicles (Fig. 3A). Intracellular Aβ(1–42)[565] could be detected after treatment with protofibrils (150 nM, Fig. 2A) or with mono-

mers at a higher concentration (500 nM, Fig. 2B). Treatment with low concentrations of monomeric Aβ(1–42)[565] (150 nM, Fig. 2C) or with an aggregation-incompetent scrambled peptide, sc-Aβ(1–42)[565] (500 nM, Fig. 2D), did not lead to detectable Aβ(1–42)[565] inclusions, as was the case for untreated cells (Fig. 2E, n.c.). Quantitative analysis of Aβ(1–42)[565] fluorescence in the endocytic vesicles and in the cytosol revealed that a low level cytosolic Aβ(1–42)[565] signal could be detected after treatment with protofibrils (150 nM) or high concentration (500 nM) monomeric Aβ(1–42) but not at low monomer concentrations (150 nM). The Aβ(1–42)[565] signal in the surrounding cytosol was about 30-fold lower than in the vesicles (Fig. 2F). The lack of uptake of sc-Aβ(1–42)[565] demonstrated that internalization was specific for the Aβ(1–42) sequence and was not a result of the fluorescent label (Fig. 2D).

We then verified that internalization of Aβ(1–42)[565] into endocytic vesicles was also observed in primary hippocampal neurons (Fig. 3, A–C). After incubating neurons with aggregated Aβ(1–42)[565] (150 nM), monomeric Aβ(1–42)[565] (150 or 500 nM), and calcein (20 μM) at 37 °C for 1 day, the uptake of Aβ(1–42)[565] and the colocalization of internalized Aβ(1–42)[565] and calcein were observed for aggregated Aβ(1–42) (Fig. 3A) and for monomeric Aβ(1–42) at 500 nM (Fig. 3B), but not for monomeric Aβ(1–42) at 150 nM (Fig. 3C), supporting our results from the neuroblastoma cell model. On the images, internalized Aβ(1–42)[565] shown in neurons (Fig. 3, A and B) and SH-EP cells (Fig. 2, A and B) seem different in quantity and distribution, which may be the result of the isolation of glia-free hippocampal neurons, or may reflect a general higher endocytic activity of neurons under the same experimental conditions.

To test whether exogenous fluorescence represented Aβ species, we co-stained cells with the anti-β-amyloid antibody 6E10, which confirmed that Atto565 fluorescence indeed indicated the presence of Aβ (Fig. 3, D and E). Conversely, 6E10 staining detected only endogenous amyloid precursor protein in the absence of Aβ(1–42)[565] (Fig. 3F). These results suggest that protofibrillar Aβ(1–42) is taken up at lower concentrations than the monomers, and that an effective uptake of monomer may require Aβ to form an ordered aggregate structure prior to cellular uptake.

*Uptake of Monomer Requires a Minimum Aβ Concentration*— To quantitatively analyze the dependence of monomer uptake on the concentration of Aβ(1–42), we titrated the cells either with Aβ(1–42) monomer or protofibrils at 15–1500 nM (equivalent monomer concentration), and quantified intracellular Aβ(1–42) as a function of Aβ(1–42) concentration by the fluorescence of labeled Aβ(1–42) using HCS microscopy (Fig. 4A).

We tracked the amount of internalized Aβ as a function of time and found maximal intracellular Aβ(1–42) signal after 24 h (Fig. 4B). The treatment with monomeric Aβ(1–42) (200 nM) did not result in cell death within 49 h (data not shown). We thus used 24 h incubation for subsequent HCS microscopy experiments. For monomeric Aβ(1–42), the total amount of intracellular Aβ(1–42) as well as the number of aggregates and their area was proportional to Aβ(1–42) monomer concentrations in the medium. No intracellular
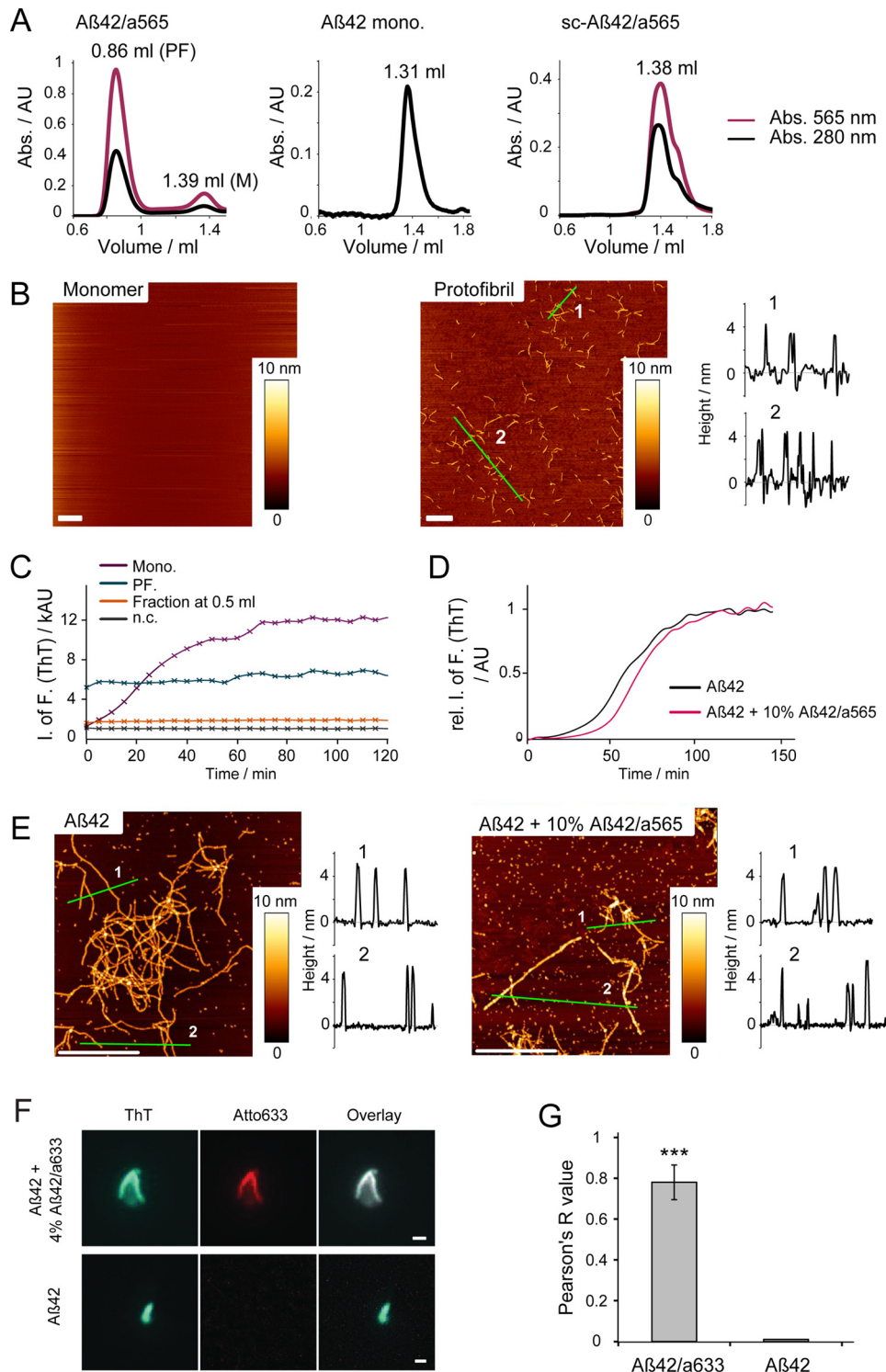
FIGURE 1. **Purification of fluorescently labeled Aβ(1–42) species.** *A,* separation of Aβ(1–42) by SEC. Labeled peptides eluted in a protofibril (*PF*) and a monomer (*M*) fraction. Peptides and labels were detected by absorption at 280 nM and 565 nm, respectively. The elution locations of monomers, Atto565-labeled Aβ(1–42) (*Aβ42/a565*), unlabeled monomeric Aβ(1–42) (*Aβ42 mono.*), and Atto565-labeled scrambled-Aβ(1–42) (*sc-Aβ42/a565*), have very similar SEC elution profiles. *B,* no aggregates were detected by AFM in the Aβ(1–42)[565] monomer fraction collected from SEC (1.39 ml). Aβ(1–42)[565] protofibrils with an average height of about 4 nm could be detected in the protofibril fraction of SEC. *C,* unlabeled monomeric Aβ(1–42) (35 μM), Aβ(1–42) protofibrils (35 μM monomer equivalent), and an elution fraction at 0.5 ml on SEC (20 μl) were incubated in PBS in presence of ThT (20 μM). ThT fluorescence of monomers displayed typical sigmoid kinetics. Protofibrils bound ThT immediately and stayed constant in fluorescence. *D,* monomeric Aβ(1–42) was mixed with 10% Aβ(1–42)[565] monomers and incubated in PBS. Aggregation was monitored by ThT fluorescence. The curves were normalized to the maximum intensity of fluorescence of plateaus. All results are represented as mean values of 3 replicate wells. *E,* unlabeled monomeric Aβ(1–42) or Aβ(1–42) mixed with 10% Aβ(1–42)[565] was incubated in PBS for 2 days. Similar fibril structures were detected in both samples. *F,* fluorescence microscopy of Aβ(1–42) aggregated in the absence or presence of 4% Aβ(1–42)[633] detected by ThT and Atto633 fluorescence. *G,* Pearson correlation analysis of ∼100 aggregates from three independent samples indicates that ThT and Atto633 fluorescence are highly correlated in labeled Aβ fibrils; all *scale bars,* 1 μm; *** indicates $p < 0.001$.
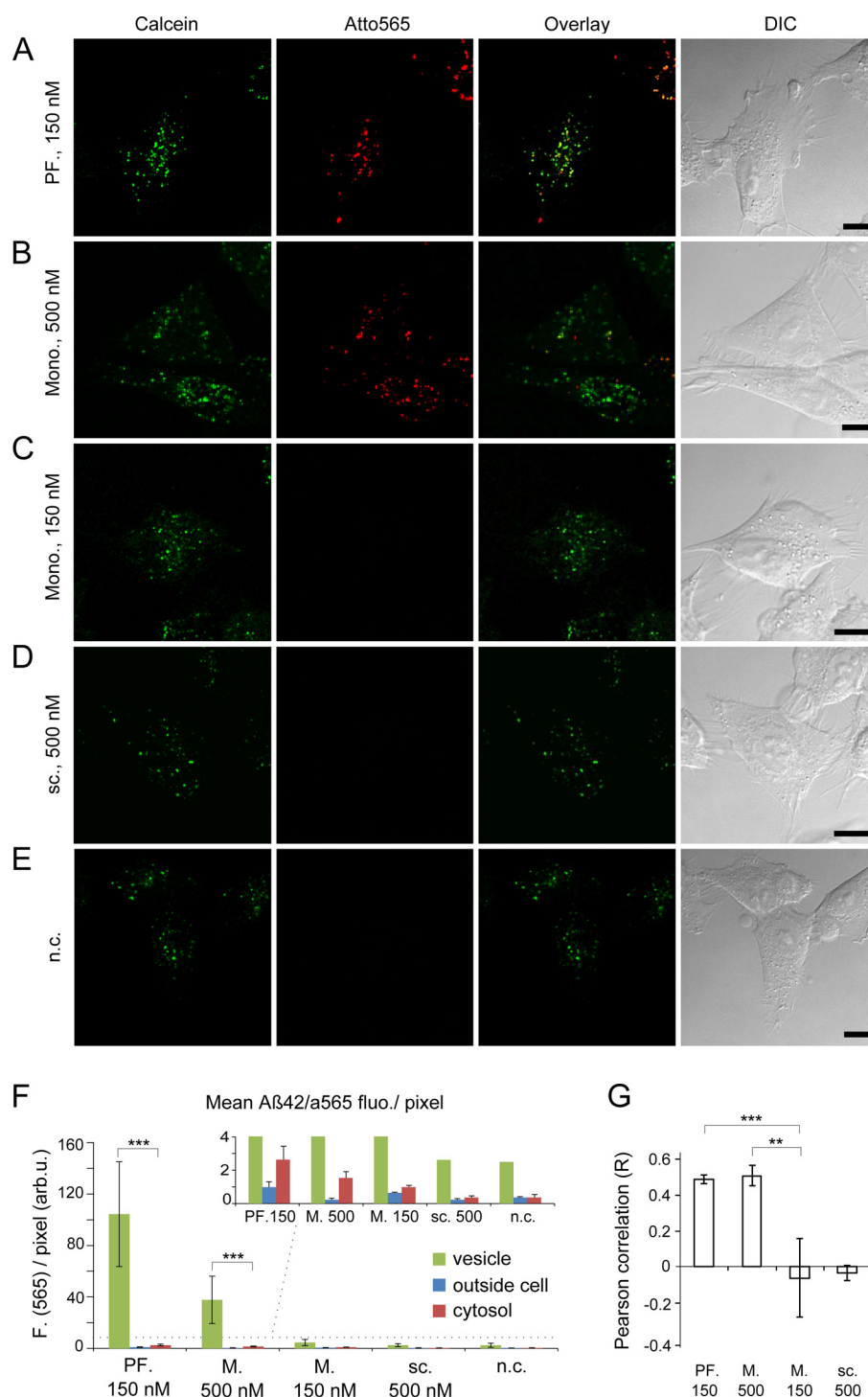
FIGURE 2. **Internalization of Aβ(1– 42) depends on aggregation states.** *A–E*, SH-EP cells were incubated with purified monomers or protofibrils at 37 °C for 24 h, and imaged by confocal microscopy, Aβ(1–42)^{565} fluorescence (*red*), calcein fluorescence (*green*). *A*, Aβ(1–42) protofibrils (*PF*, 150 nM); *B*, monomeric Aβ(1–42) (*M*, 500 nM); *C*, monomeric Aβ(1–42) (*M*, 150 nM); *D*, sc-Aβ(1–42)^{565} (*sc*, 500 nM); and *E*, negative control (*n.c.*). *Scale bars,* 10 μm. *F*, average fluorescence intensities per pixel inside endocytic vesicles, in the cytosol and in the extracellular space were calculated from the 565 nm channel of confocal images in *A–E*. *Bar graphs* represent average values ± S.D. from image areas corresponding to endocytic vesicles marked by calcein (*n* = 10), or from areas in the cytosol without vesicles (*n* = 3) or in the extracellular space (*n* = 3), respectively. Only cells treated with aggregated Aβ(1–42)^{565} (150 nM; *PF, 150*) or monomeric Aβ(1–42)^{565} (500 nM; *M.500*) displayed fluorescence above the background of untreated cells (*n.c.*), whereas those treated with Aβ(1–42)^{565} monomers at 150 nM (*M.150*) and sc-Aβ(1–42)^{565} (500 nM; *sc.500*) did not. *Inset*, cells treated under conditions that resulted in uptake of Aβ(1–42)^{565} aggregates displayed a 3-fold increase in cytosolic Aβ(1–42)^{565} signal compared with the extracellular space. Aβ(1–42)^{565} fluorescence in the cytosol is ~30-fold lower than inside the vesicles. *G*, Pearson correlation analysis of colocalization between calcein and Aβ(1–42)^{565} fluorescence in *panels A–E*. *Bars* indicate average *R* values of three regions of interest ± S.D., ***, indicates *p* < 0.001; **, *p* < 0.007.

Aβ(1– 42) was observed at concentrations of 150 nM and below (Fig. 4, *C* and *D*). In contrast, no such threshold concentration existed for the internalization of preformed

Aβ(1– 42)^{565} aggregates (Fig. 4, *E* and *F*). The observed threshold concentration for monomer uptake is similar to the critical concentration (22) that was reported for the
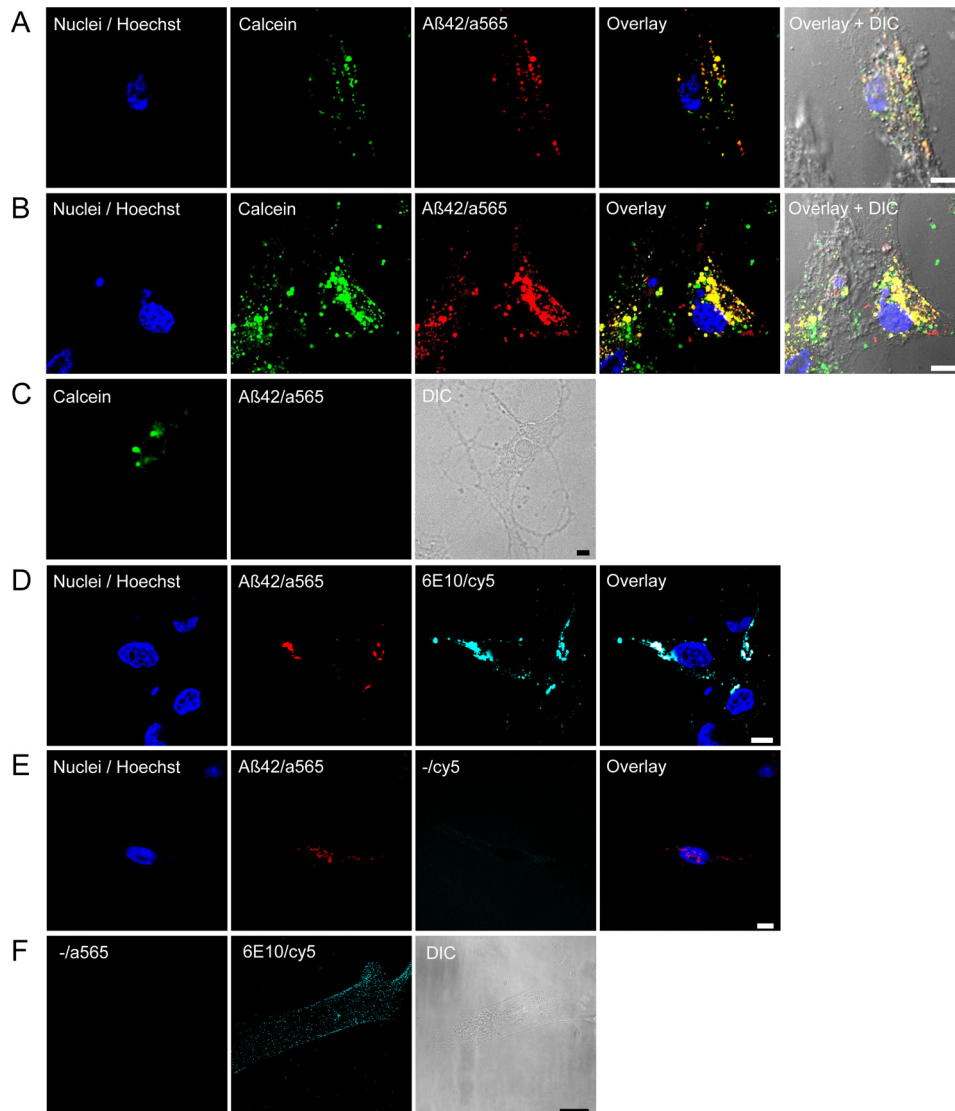
FIGURE 3. **Internalization of Aβ(1–42) by primary neurons and immunofluorescence staining of internalized Aβ(1–42).** *A–C*, primary hippocampal neurons incubated with pre-aggregated Aβ(1–42)[565] at 150 nM (*A*), monomeric Aβ(1–42)[565] at 500 nM (*B*), or monomeric Aβ(1–42)[565] at 150 nM concentration (*C*). Nuclei were stained by Hoechst 33342 (*blue*), endocytic vesicles were stained with calcein (*green*). *D–F*, co-staining of the internalized Aβ(1–42) with anti-β-amyloid antibody. SH-EP cells were incubated with Aβ(1–42)[565] (500 nM, equivalent monomer concentration) (*D* and *E*), or Atto 565 dye (*F*) at 37 °C for 24 h. Fixed cells were co-stained by anti-Aβ antibody (6E10) by IF staining, visualized by Cy5-conjugated secondary antibody (*cyan*), and imaged by confocal microscopy. Cell nuclei were stained with Hoechst 33342 (*blue*). *D*, internalized Aβ(1–42)[565] was co-stained by 6E10/Cy5. *E*, no secondary antibody bound without primary antibody (6E10) to Aβ(1–42)[565]. *F*, Atto565 dye was not taken up, and 6E10/Cy5 did not mark dye molecules; *scale bars,* 10 μm.

aggregation of Aβ(1–42) monomers, which suggests that aggregation may be a prerequisite for uptake.

Alternatively, differences in the degradation of Aβ(1–42) by proteases, either extracellular prior to uptake or intracellular, could cause the higher amount of Aβ(1–42) in the cells. To test this alternative hypothesis, we monitored concentrations of Aβ(1–42) in the cell culture media and in cell lysates as a function of time by immunoblotting (Fig. 4, *G* and *H*). We observed a pronounced increase of Aβ(1–42) in the lysates of cells incubated with aggregated Aβ(1–42) (500 nM) and a smaller increase in cells incubated with monomer (500 nM) after 24 h, mirroring the results from HCS microscopy (Fig. 4*B*). We then monitored the Aβ(1–42) concentration in the culture media, either in the presence of cells or in control samples that were incubated without cells for 24 h. When monitoring the Aβ(1–42) concentration in the culture media, no decrease of Aβ(1–

42) over time was observed for monomeric Aβ(1–42) in the presence of cells or for either form of Aβ(1–42) in the control samples without cells. These data indicate that monomeric Aβ(1–42) is not degraded by proteases in the media, which would prevent its uptake. Rather, only the concentrations of aggregated Aβ(1–42) were reduced substantially over time, likely reflecting its more efficient binding to, and uptake into cells. Taken together, these data strongly support our initial hypothesis that uptake of Aβ(1–42) does indeed depend on its aggregation state. If so, it would be important to determine the type of aggregates that are efficiently taken up by the cells.

Efficient Uptake Correlates with Formation of β-Sheet-rich Aggregates—To determine which Aβ species could be efficiently taken up, we combined *in vitro* aggregation kinetics and cellular uptake experiments. Aβ(1–42) amyloid formation was monitored *in vitro* to collect Aβ(1–42) species at different
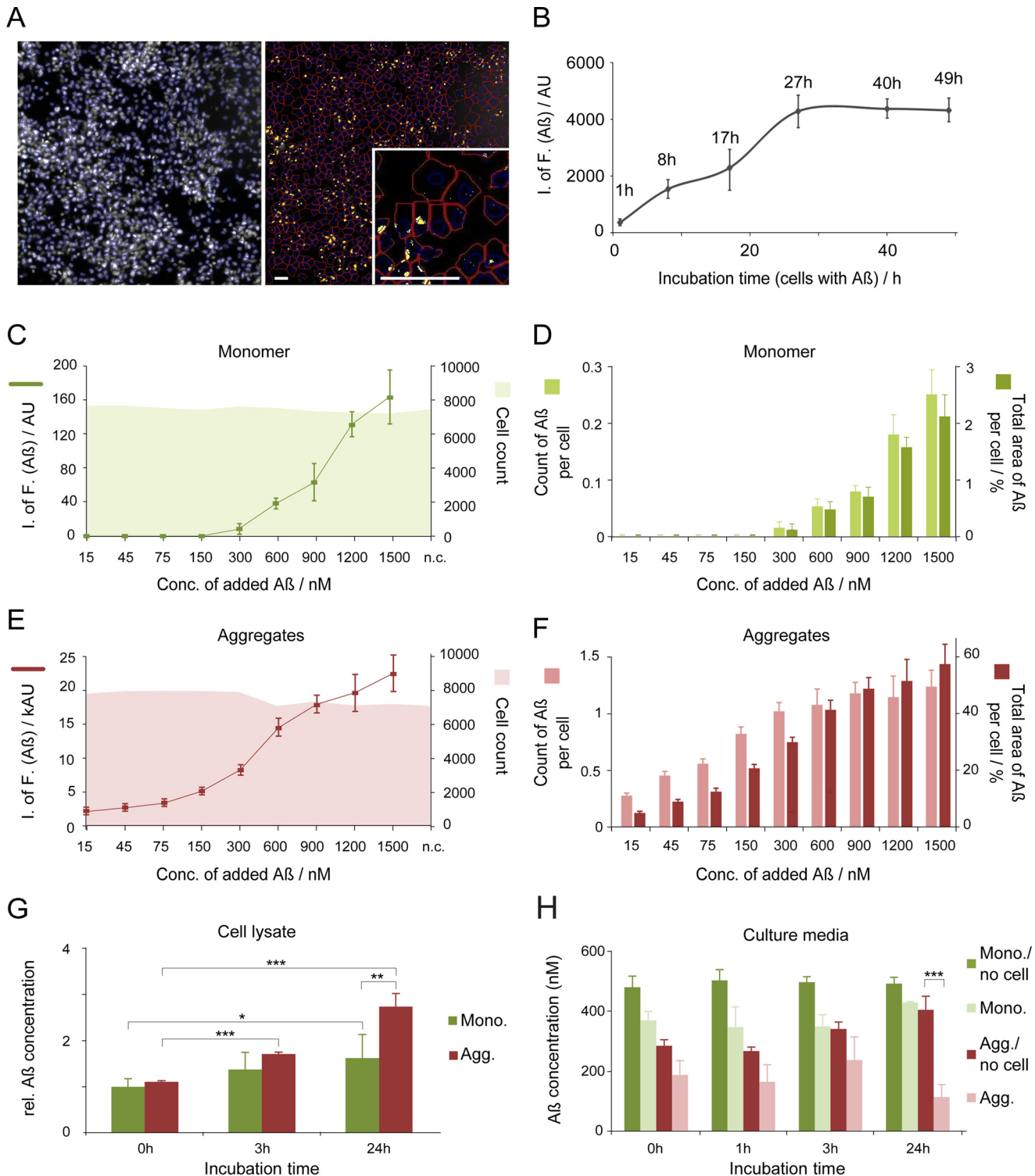
FIGURE 4. **Internalization of Aβ(1–42) depends on concentration.** *A,* HCS microscopic images of SH-EP cells with Aβ(1–42)[565] aggregates. *Left,* cell nuclei were stained with Hoechst 33342 (*white*). Nuclei, which locate in focus plane, were identified by the image analysis software (*blue contour lines*). *Right,* the software identification of nuclei (*blue contour lines*) in the cell bodies (*red contour lines*) and Aβ(1–42)[565] aggregates inside the cell bodies (*yellow spots*); *scale bars,* 100 μm. *B,* SH-EP cells were incubated with purified Aβ(1–42)[565] monomer (200 nM) at 37 °C from 1 to 49 h. Intracellular Aβ(1–42)[565] in fixed cells was analyzed by HCS microscopy. Maximal intracellular Aβ(1–42) was reached after 27 h. *C–F,* SH-EP cells were incubated with Aβ(1–42)[565] monomer (*C* and *D*) or aggregates (*E* and *F*) at 37 °C for 24 h. Total fluorescence intensities Aβ(1–42)[565], cell number per well, the number of Aβ(1–42)[565] aggregates per cell, and total aggregates area were plotted as functions of Aβ(1–42)[565] concentration. All results are represented as mean ± S.D. of 6 replicate wells. *G* and *H,* quantification of Aβ(1–42) of SH-EP cells incubated with Aβ(1–42) monomer (500 nM) or aggregates in cell lysates (*G*) and cell culture media by dot blotting (*H,* mAb 6E10). Differences between 0, 1-, 3-, and 24-h incubation samples incubated under the same conditions were not statistically significant. *Bars* represent mean ± S.D. of three replicate wells; *** indicates $p < 0.001$; ** indicates $p < 0.003$; * indicates $p < 0.05$.
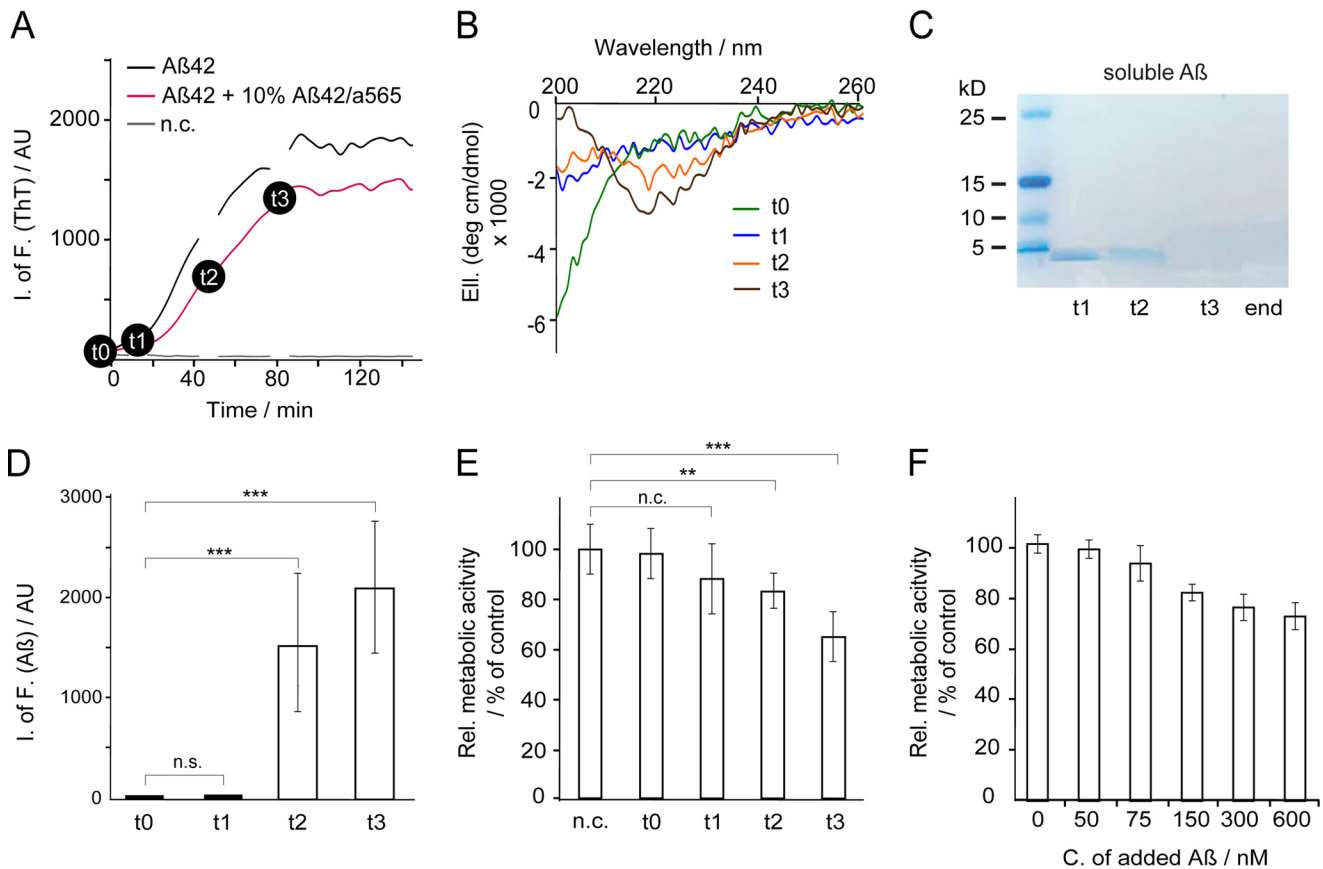
FIGURE 5. **Aβ(1–42) uptake of β-sheet structures.** *A,* aggregation kinetics of monomeric Aβ(1–42) (15 μM) with 10% Aβ(1–42)[565] in PBS were monitored by ThT fluorescence. Aggregates were collected from the aggregation assay at four time points (t0–t3). *B,* Aβ(1–42) secondary structure was measured by circular dichroism spectroscopy. *C,* quantification of soluble Aβ(1–42) by SDS-PAGE and Coomassie staining after ultracentrifugation for 30 min at 200,000 × *g*. *D,* Aβ (t0–t3) was diluted to a final concentration of 150 nM added to SH-EP cells for 24 h incubation time. Internalized Aβ(1–42)[565] was quantified by HCS microscopy of fixed cells. *E,* metabolic activities of SH-EP cells treated with Aβ (150 nM, t0–t3) or untreated cells (*n.c.*). After 1 day of incubation, metabolic activities were monitored by MTT assay. *F,* metabolic activities of SH-EP cells treated with monomeric Aβ at 0–600 nM. After 1 day, the toxicity was monitored by MTT assay. All results are represented as mean ± S.D. of three replicate wells for ThT kinetics (*A*), of 6 replicate wells for uptake (*D*) and 12 replicate wells for MTT assays (*E* and *F*); *** indicates $p < 0.001$, ** indicates $p < 0.003$; *n.s.*, not significant.

stages of aggregation. Then their uptake was monitored through the fluorescence of labeled Aβ(1–42).

Aβ(1–42) (15 μM, 10% Aβ(1–42)[565]) aggregation kinetics were monitored by ThT fluorescence (Fig. 5*A*). Samples were collected at four time points that corresponded to different phases of peptide aggregation: initiation (t0), lag-phase (t1), growth phase (t2), and plateau phase (t3). The samples were characterized by CD spectroscopy (Fig. 5*B*). Within the lag phase (t0 and t1), Aβ(1–42) partially lost its disordered state. It adopted a β-sheet structure during the growth phase (t2 and t3) as indicated by a minimum at 218 nm in the CD spectra. When centrifuged at 200,000 × *g*, soluble Aβ(1–42) was lost during its growth phase (t2–t3, Fig. 5*C*). To determine which of these aggregation states are efficiently taken up, the SH-EP cells were incubated with Aβ species (t0–t3) at 37 °C at 150 nM equivalent monomer concentration, which is below the threshold concentration of Aβ(1–42)[565] monomer internalization (Fig. 4*D*). After 24 h incubation, intracellular Aβ(1–42) aggregates were quantified by HCS microscopy (Fig. 5*D*). Intracellular Aβ(1–42)[565] aggregates were detected in cells that had been treated with growth (t2) and the steady-state phase (t3) aggregates. In contrast, no uptake of Aβ(1–42) peptides was observed with samples from the initiation (t0) and lag phase (t1) of the poly-

merization reaction. This suggests that β-sheet-rich Aβ(1–42) aggregates are efficiently internalized, whereas unstructured monomers (t0) or small aggregates/oligomers (t1) without β-sheet structure are not.

HCS data from Fig. 4, *C* and *E*, show that neither form, monomer or small aggregates, had a strong effect on the number of living cells, *i.e.* internalized Aβ(1–42)[565] did not cause cell death within 24 h. We therefore analyzed cell metabolic activities by 3-(4,5-dimethylthiazol-2-yl)-2,5-diphenyltetrazolium bromide (MTT) reduction, which is a well established marker of early mitochondrial toxicity (23).

Aβ(1–42) aggregates formed during the growth phase (t2 and t3) were significantly more toxic than monomers (t0) and samples collected during the lag-phase (t1) and inhibited mitochondrial metabolic activity (Fig. 5*E*). Under our experimental conditions Aβ(1–42) monomers became cytotoxic only at concentrations above 150 nM (Fig. 5*F*), a point at which they also underwent internalization (Fig. 4, *C* and *D*).

It should be noted that the dilution to 150 nM might change the structure of Aβ(1–42) in the medium from the structure recorded by CD at 15 μM (Fig. 5*B*). Nevertheless, at concentrations of 150 nM and below only Aβ(1–42) that had previously formed β-sheet-rich structures (t2, t3) was efficiently internal-

ized, whereas unstructured monomers (t0) or small aggregates (t1) without β-sheet structure were not. This suggests that it was indeed the β-sheet aggregates that were taken up, rather than a different Aβ(1–42) species. The question whether the intracellular Aβ(1–42) still had β-sheet structure will be addressed in detail below.

These data support the hypothesis that the formation of a β-sheet structure may be a prerequisite for efficient uptake and subsequent cytotoxicity of Aβ(1–42) aggregates in neuronal model cells. The results raise the question where Aβ(1–42) aggregates form. Aggregation could occur in the medium or, alternatively, the cellular membrane may serve as a platform for the aggregation process.

Multimerization on Plasma Membrane Precedes Uptake of Aβ(1–42)—To investigate the location of aggregate formation and to better track the dynamics of monomer uptake, we repeated the uptake experiment under conditions that allowed us to separate in time Aβ(1–42) membrane interaction from its uptake into the cell. The cells were cooled to 4 °C, which slows down both Aβ(1–42) aggregation and cell metabolism, and then were treated with Aβ at 4 °C for 45 min. The cells were then washed with ice-cold PBS to remove unbound Aβ(1–42), and then restored at 37 °C in fresh media (Fig. 6A).

Under these conditions (4 °C, 60 min), even at a higher monomer concentration of 1 μM, Aβ(1–42)[565] was located only on the plasma membrane and no uptake could be observed (Fig. 6B). Calcein (20 μM) uptake displayed that the cell still had some endocytic activity under these conditions.

First, we tested whether monomeric Aβ(1–42) assembles into larger species on the cell membrane. We incubated SH-EP cells with two types of fluorescently labeled monomeric Aβ(1–42), Aβ(1–42)[488], and Aβ(1–42)[633]. The self-assembly of Aβ(1–42) into di- and multimeric species was quantified by FRET between both fluorophores. After preincubation at 4 °C for 15 min, SH-EP cells were treated with monomeric Aβ(1–42)[488] and Aβ(1–42)[633] (500 nM total Aβ(1–42) concentration) at 4 °C for 45 min. Confocal imaging showed that both Aβ(1–42)[488] and Aβ(1–42)[633] accumulated at the plasma membrane (Fig. 6C). Aβ(1–42)[488] and Aβ(1–42)[633] not only colocalized but also displayed a FRET signal, indicating direct interaction between the two-labeled Aβ(1–42) species. These data demonstrate that at least a fraction of the monomeric Aβ(1–42) peptides rapidly co-aggregated on the plasma membrane.

We then tested if those membrane-bound Aβ(1–42) aggregates did indeed form on the plasma membrane and could be taken up after their aggregation. To do so, SH-EP cells were treated successively with monomeric Aβ(1–42)[488] and Aβ(1–42)[633], each at 500 nM concentration. SH-EP cells were first only incubated with monomeric Aβ(1–42)[488] at 4 °C for 30 min, which was then washed off. After removing the unbound Aβ(1–42)[488], the cells were treated with Aβ(1–42)[633] at 4 °C for another 30 min. After that, the cells were washed again to remove unbound Aβ(1–42), incubated in fresh medium at 37 °C for 3 h to permit internalization of Aβ(1–42), and imaged by confocal microscopy (Fig. 6D). Both labeled Aβ(1–42) species colocalized in the endocytic vesicles. The FRET signal indicates that both had formed di- or multimeric complexes. Because the washing step had removed all Aβ(1–42)[488] from

solution, we conclude that Aβ(1–42)[488] interacted with Aβ(1–42)[633] while located on the plasma membrane. The membrane-bound aggregates were then taken up by endocytosis after the cells were returned to 37 °C.

To verify that the FRET signal is specific to physical interaction of Aβ(1–42) monomers and is not an artifact of the label or of colocalization, we used transferrin (Tf) as a negative control. Tf binds to a membrane receptor and is internalized via clathrin-mediated endocytosis but does not aggregate on the membrane. After incubating the cells at 4 °C with two types of fluorescent transferrin conjugates (Tf/A488 and Tf/A647), we observed colocalization of both Tf conjugates. However, the colocalization did not correspond to a FRET signal (Fig. 6E). This strongly suggests that the FRET between Aβ(1–42) molecules results from a specific physical interaction.

For a more comprehensive analysis of the membrane-assisted self-assembly and subsequent uptake of Aβ(1–42) monomers, the cells were treated with monomeric Aβ(1–42)[565] at various concentrations (0–1600 nM) at 4 °C for 45 min. Subsequently the temperature was raised to 37 °C to permit internalization of Aβ(1–42) and the cells were incubated in fresh medium for 24 h. Intracellular Aβ(1–42)[565] was then quantified by HCS microscopy (Fig. 6F). Intracellular Aβ(1–42)[565] aggregate signals could be detected at Aβ(1–42)[565] monomer concentrations above 200 nM, similar to the threshold concentration we previously observed for monomer uptake at 37 °C (Fig. 4, B and C). These data demonstrate that Aβ(1–42) binds to the plasma membrane and forms aggregates prior to cellular uptake, that the cell membrane assisted Aβ(1–42) self-assembly, and that uptake of monomeric Aβ(1–42) requires a critical Aβ(1–42) concentration for membrane-assisted uptake.

Conceivably, small Aβ(1–42) aggregates that are competent for uptake could be forming in solution and then bind to the plasma membrane. However, a comparison of conditions and time scales of Aβ(1–42) aggregation in solution with those of the membrane binding experiment makes this hypothesis less likely. Incubation of cells with Aβ(1–42) monomer for 45 min at 500 nM was sufficient to initiate uptake. In contrast, ThT positive Aβ(1–42) species did not form in solution under the same conditions within 3 h even at monomer concentrations of 1500 nM (Fig. 6G).

Finally, we probed the complex formation of Aβ(1–42)[488] and Aβ(1–42)[633] (150 nM each) by FRET as a function of time (Fig. 6H). Little FRET signal was observed within the first 3 h, supporting our conclusion that membrane binding coincides with, or precedes interaction at this peptide concentration. Conversely, no FRET signal was observed after the co-incubation of scrambled sc-Aβ(1–42)[488] and Aβ(1–42)[633] (150 nM each), reinforcing that interaction depends on the Aβ peptide sequence and not on the fluorescent label. Formation of FRET-positive species also coincided with the time course of Aβ aggregation *in vitro* (Fig. 6, G and H), suggesting that the FRET signal results from multimeric aggregated Aβ species.

We therefore conclude that binding to the plasma membrane occurred within the lag-phase of ThT aggregation kinetics, well before the formation of β-sheet-rich aggregates. Because our previous experiment demonstrated that formation of β-sheet
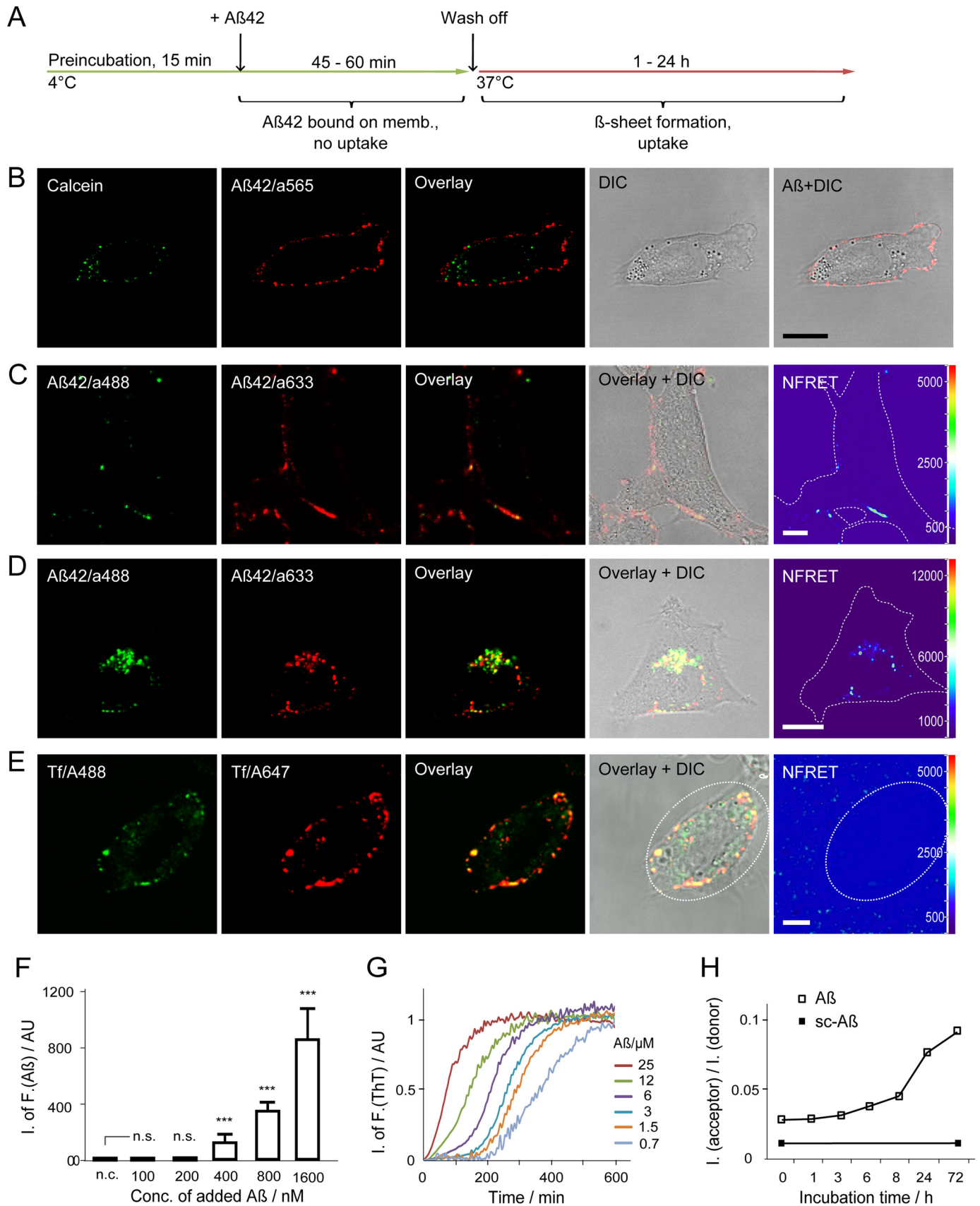
structures *in vitro* correlated with efficient uptake (Fig. 5, *B* and *C*), these data suggest that Aβ(1–42) peptides may convert into β-sheet aggregates on the membrane prior to uptake after soluble Aβ(1–42)[565] peptides were removed. We therefore analyzed, whether intracellular Aβ(1–42) contained β-sheet structures.

Internalized Aβ(1–42) Contains β-Sheet-rich Structures—To identify the secondary structure of internalized Aβ(1–42) in the cultured cells, we stained cells with the amyloidophilic dye ThS and the anti-amyloid fibril antibody LOC after Aβ(1–42) uptake. ThS is widely used to visualize β-sheet-rich amyloid structures in histology (20, 24). It displays enhanced fluorescence emission on β-sheet binding, and has higher affinity and less pH sensitivity than ThT (20). When pre-aggregated Aβ(1–42) (t1–t3) is taken up, both ThS and LOC staining colocalize with Aβ(1–42)[633] fluorescence confirming the presence of fibrillar aggregates (Fig. 7, *A* and *B*). However, ThS and LOC signals after incubation with monomeric Aβ(1–42) do not clearly demonstrate the presence of β–sheet rich fibrils (Fig. 7, *A* and *B*). This leaves open the possibility that the Aβ(1–42) species detected by FRET have not yet formed β-sheet structures.

Our previous experiments found: (i) monomeric Aβ(1–42) is internalized at concentrations above ~200 nM; (ii) Aβ(1–42) aggregates on the plasma membrane; and (iii) aggregates containing β-sheet structure were taken up very efficiently, all suggesting a conversion of monomeric Aβ(1–42) into β-sheet structure during uptake.

To resolve whether this conversion occurs, we performed a competitive uptake experiment between monomer at a subcritical concentration (Aβ(1–42)[565], 150 nM), which was co-incubated with β-sheet aggregates (Aβ(1–42)[633], 900 nM). Both species were labeled with different fluorophores to track in which compartment both monomers and aggregates were found. In addition, β-sheet-rich structures were stained by ThS. According to our previous results, we would expect monomers to be taken up only if they converted into β-sheet structures via co-aggregation with pre-formed aggregates and that internalized Aβ(1–42) co-stains with ThS.

SH-EP cells were treated with Aβ(1–42)[565] monomer (150 nM) at 4 °C for 20 min. Monomeric Aβ was removed, and then cells were treated with Aβ(1–42)[633] aggregates at 900 nM at 4 °C for 20 min, washed with ice-cold cell culture medium, and stained with ThS at 4 °C for 10 min. After that, the cells were further incubated in fresh cell culture medium with calcein (20 μM) at 37 °C for 1 h. After removing the calcein-rich medium,

the cells were incubated in calcein-free medium at 37 °C, and live cell images were taken by spinning disk confocal microscopy (Fig. 7*C*).

Aβ(1–42)[565] was observed in both states, ThS positive (Fig. 7*C*, *circle 1*) and ThS negative (Fig. 7*C*, *circles 2* and *3*). In Fig. 7*C*, *circles 1* and *2* show two structures that contained both Aβ(1–42)[565] and Aβ(1–42)[633]. However, only the ThS positive structure colocalized with calcein (Fig. 7*C*, *circle 1*). In contrast, ThS negative structures did not colocalize with calcein and were thus not inside the endocytic vesicles (Fig. 7*C*, *circle 2*). We quantified ThS fluorescence of Aβ(1–42)[565] monomers that colocalized with Aβ(1–42)[633] fibrils and with Aβ(1–42)[565] structures that did not contain Aβ(1–42)[633] (Fig. 7*D*). Only Aβ(1–42)[565] that had coaggregated with Aβ(1–42)[633] fibrils (Fig. 7*D*, F(fibril)/F(mono) >5) stained strongly with ThS ($p < 0.008$). In contrast, Aβ(1–42)[565] that had not coaggregated with Aβ(1–42)[633] fibrils (Fig. 7*D*, F(fibril)/F(mono) < 5) did not colocalize with ThS. Aβ structures that did not colocalize with ThS were not internalized (Fig. 7*C*, *circle 3*).

We quantitatively analyzed internalized and surface-bound species of monomeric Aβ from confocal live cell imaging (Fig. 7*E*). All monomeric Aβ found inside the cell both colocalized with preaggregated Aβ fibrils and stained strongly with ThS, whereas ~⅓ of surface-bound monomeric Aβ did not colocalize with fibrillar Aβ or stained with ThS. We did not find any monomeric Aβ that stained with ThS without colocalizing with fibrillar Aβ either inside the cells or on the cell surface under these experimental conditions.

This means that subthreshold concentrations of Aβ(1–42) monomers were capable of binding to the plasma membrane. However, co-aggregation into β-sheet-rich structures was needed for their efficient uptake into the cells.

Finally, we monitored the incorporation of Aβ monomers into β-sheet-rich aggregates on the surface of SH-EP cells by live cell FRET imaging (Fig. 7*F*, supplemental Fig. S1). Monomeric Aβ coaggregated with Aβ fibrils within 30 min into structures that also bound ThS. Taken together, these data strongly support our hypothesis, that aggregation into β-sheet structures facilitates the efficient uptake of Aβ(1–42) by neuroblastoma cells via an endocytic mechanism.

Aβ(1–42) Aggregate Uptake Is Clathrin Independent—The location of Aβ(1–42) aggregates in endocytic vesicles raises the question by which endocytic pathway β-sheet-rich aggregates are internalized. Here we tested whether Aβ(1–42) aggregates are internalized by clathrin-mediated endocytosis (CME). The CME pathway was blocked by lowering the temperature to 4 °C

FIGURE 6. **Aggregation of Aβ(1–42) occurs on the plasma membrane.** *A*, experimental scheme. SH-EP cells were incubated with monomeric Aβ(1–42) at 4 °C, then cells were either imaged directly or Aβ(1–42) was washed off, the cells were further incubated in fresh medium at 37 °C. Intracellular Aβ(1–42) was quantified by confocal microscopy or HCS microscopy. At 4 °C, Aβ(1–42) monomers bound only to the plasma membrane, and at 37 °C endocytosis of Aβ(1–42) aggregates occurred. *B*, after incubating with monomeric Aβ(1–42)[565] (1 μM) and calcein (20 mM) at 4 °C for 60 min, Aβ(1–42) was located only at the plasma membrane of SH-EP cells, no uptake could be observed. *C*, SH-EP cells were incubated with monomeric Aβ(1–42) (500 nM total Aβ(1–42)) at 4 °C for 45 min. Aβ(1–42)[488] to Aβ(1–42)[633] FRET indicated aggregates species bound to the plasma membrane. *D*, SH-EP cells were treated successively with monomeric Aβ(1–42)[488] and Aβ(1–42)[633] (each 500 nM in the medium) at 4 °C for 30 min, then incubated in fresh medium at 37 °C for 3 h. Colocalization and Aβ(1–42)[488] to Aβ(1–42)[633] FRET indicates that internalized Aβ(1–42) was in an aggregated form. *E*, SH-EP cells were incubated with transferrin/Alexa 488 (*Tf/A488*, 5 ng/ml) and transferrin/Alexa 647 (*Tf/A647*, 10 ng/ml) at 4 °C for 45 min. No FRET occurred between colocalized transferrin conjugates. Cells are marked by *white outlines* in FRET panels. *F*, SH-EP cells treated with monomeric Aβ(1–42)[565] (0–1600 nM at 4 °C for 45 min) were then incubated in fresh medium at 37 °C for 24 h. Intracellular Aβ(1–42) was quantified by HCS microscopy; *** indicates $p < 0.001$. *G*, normalized concentration-dependent Aβ(1–42) (0.7–25 μM) aggregation kinetics monitored by ThT fluorescence *in vitro*. ThT positive β-sheet structures were formed after ~3 h at 700 nM. *Scale bars*, 10 μm. All results are represented as mean ± S.D. of 6 replicate wells for uptake (*a*) and of three replicate wells for ThT kinetics. *H*, FRET signal $I_{acceptor}$ (645 nm)/I_{donor} (530 nm) of Aβ(1–42)[488] to Aβ(1–42)[633] FRET pair (150 nM each) or sc-Aβ(1–42)[488]/Aβ(1–42)[633] mixtures (150 nM each) incubated in PBS after excitation at 488 nm.
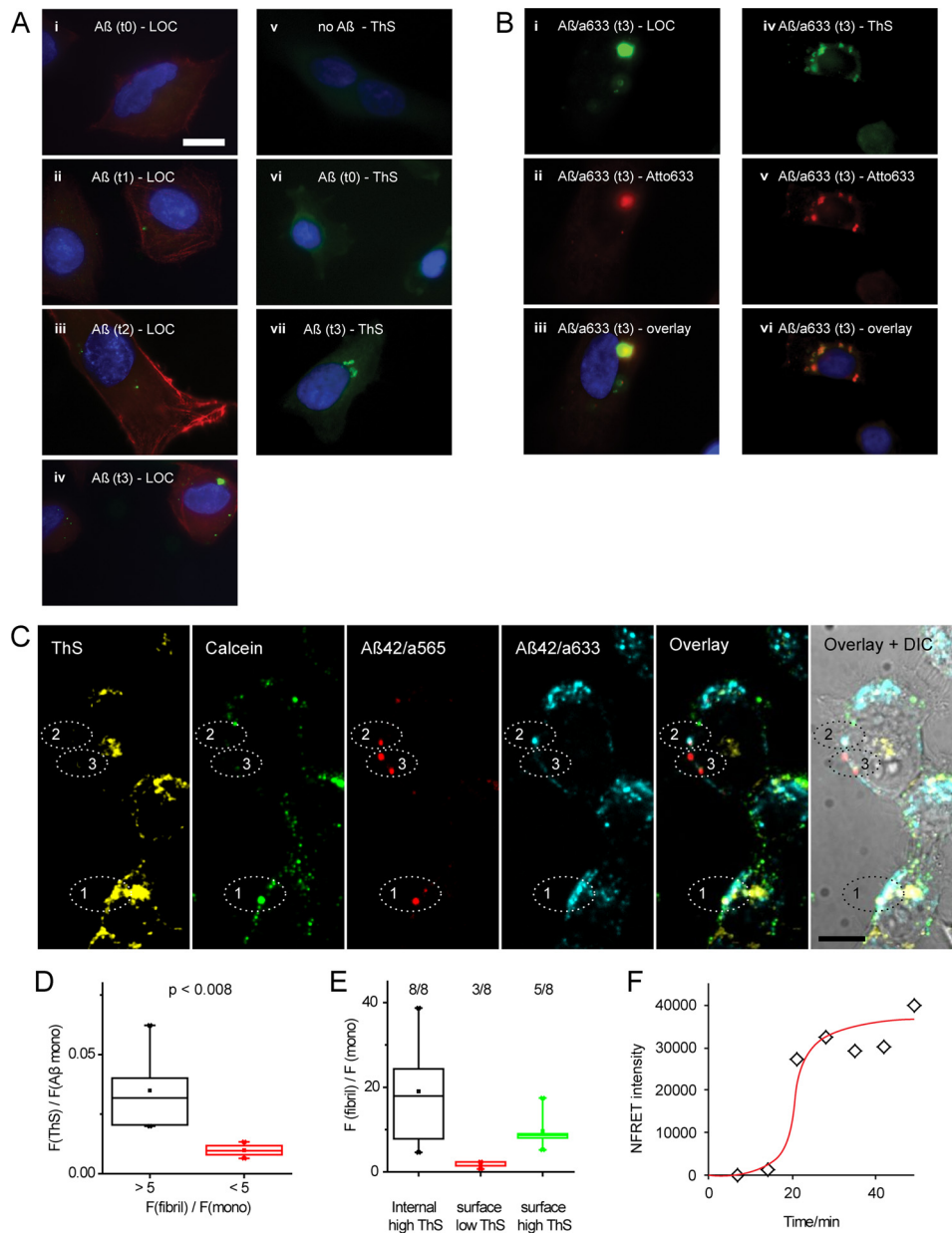
FIGURE 7. **Internalized Aβ(1–42) contains β-sheet-rich structures.** *A,* anti-amyloid fibril antibody (*LOC*) and thioflavin S (*ThS*) staining of internalized Aβ(1–42). SH-EP cells were incubated with aggregation time points (t0–t3; see Fig. 5*A*) of Aβ(1–42) (300 nM) for 3 h, after which Aβ(1–42) was removed and the cells were washed and cultivated overnight, fixed, and stained. Internalized Aβ(1–42) was stained with LOC (*i–iv, green*) or ThS (*v–vii, green*). The cell cytoskeleton was stained with phalloidin-568 (*red*) in *panels i–iv. B,* fluorescence of internalized Aβ(1–42)^{633} (*t3,* 150 nM) incubated for 6 h colocalized with ThS and LOC signals; *scale bar,* 10 μm for all panels. *C,* live cell imaging of internalized Aβ(1–42). SH-EP cells were treated with Aβ(1–42)^{565} monomer (150 nM) and Aβ(1–42)^{633} aggregates (*t3,* 900 nM), at 4 °C for 20 min each and stained with ThS. After removing unbound Aβ(1–42), the cells were incubated with calcein (20 μM) at 37 °C for 1 h. The live cell image was recorded by spinning disk confocal microscopy. Internalized aggregates that contained β-sheet structures showed positive ThS staining and positive calcein signals (*circle 1*). ThS negative Aβ(1–42)^{565}, colocalized with Aβ(1–42)^{633} (*circle 2*) or by itself (*circle 3*), was not taken up into endocytic vesicles and did not colocalize with calcein; *scale bar,* 10 μm. *D,* box plot of colocalization of monomeric Aβ(1–42)^{565} with ThS in structures that either did or did not contain fibrillar Aβ(1–42)^{633}. Only Aβ(1–42)^{565} that had coaggregated with fibrillar Aβ(1–42)^{633} stained with ThS; $n = 10$, $p < 0.008$. *E,* degree of colocalization of surface-bound and internalized Aβ(1–42)^{565} monomer with Aβ(1–42)^{633} fibrils. *F,* NFRET analysis of monomeric Aβ(1–42)^{555} (150 nM) and fibrillar Aβ(1–42)^{633} (150 nM) coaggregation in SH-EP cells acquired by sensitized emission of live cell images by confocal microscopy.

(25). Transferrin binds to the transferrin receptor on the plasma membrane and then can be internalized via coated pits. Fluorescent transferrin conjugates are therefore broadly used as markers for investigating the early phase of CME (25–28). At 4 °C, transferrin only binds to its receptor on the plasma membrane, and will not be taken up (25). Therefore, transferrin was used as specifically reported for inhibition of the CME pathway. However, it should be noted that at this temperature the fluidity

of membrane is limited, which may also influence other endocytic mechanisms or the aggregation of Aβ(1–42) (29, 30).

Following incubation with monomeric and pre-aggregated Aβ(1–42)^{565} (150 nM, respectively) calcein (20 μM) and transferrin (10 ng/ml) at 4 °C for 45 min, SH-EP cells were fixed and imaged by confocal microscopy (Fig. 8, *A* and *B*). Transferrin was located exclusively at the cell membrane, demonstrating that CME was efficiently inhibited. Under these conditions
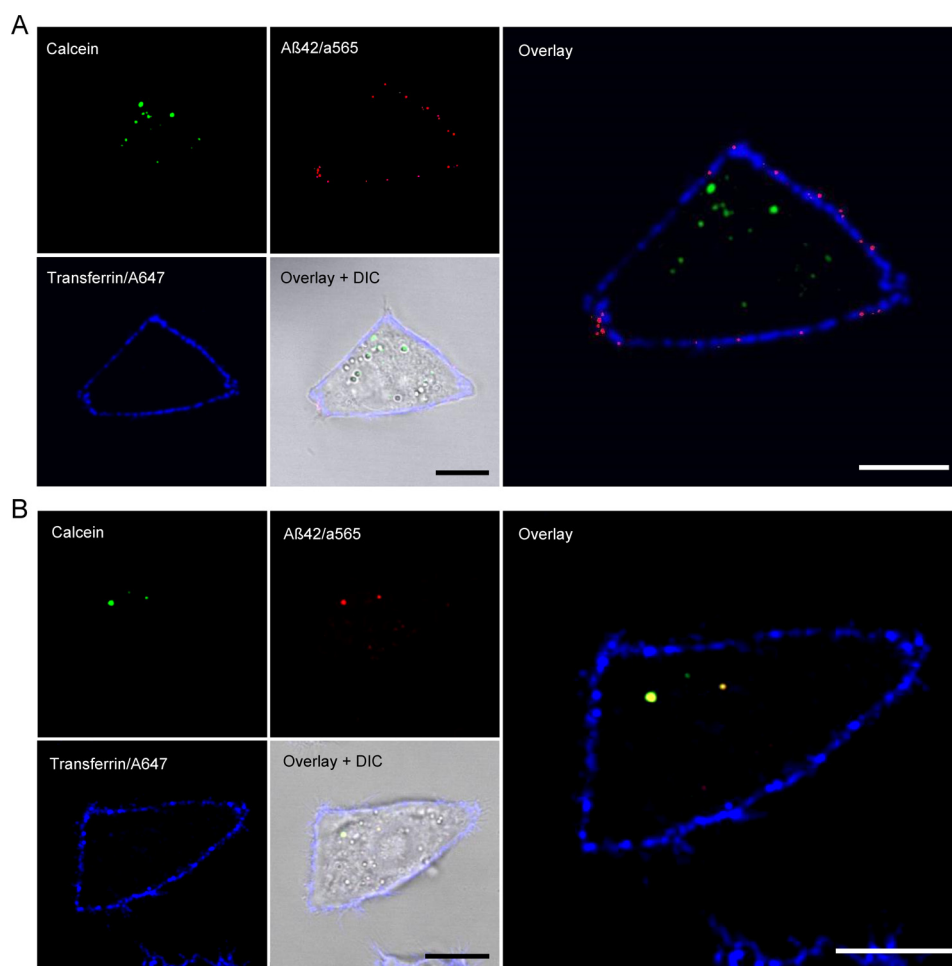
FIGURE 8. **SH-EP cells were incubated with monomeric (*A*) or pre-aggregated (*B*) Aβ(1–42)^{565} (150 nM, *red*), calcein (20 μM, *green*), and transferrin (10 ng/ml, *blue*) for 45 min at 4 °C, and were imaged by confocal microscopy.** Transferrin and Aβ(1–42) monomer was observed in the plasma membrane. Aβ(1–42) aggregates could be detected inside the cells. *Scale bars*, 10 μm.

Aβ(1–42) monomer was only observed on the plasma membrane and was not internalized. However, the Aβ(1–42) on the membrane did not colocalize with transferrin. The uptake of pre-aggregated Aβ(1–42) species was reduced but not totally inhibited under these conditions (Fig. 8*A*). However, Aβ(1–42) found in endocytic vesicles also did not colocalize with transferrin. These data suggest that uptake of Aβ(1–42) is independent of CME.

We then analyzed the internalization of Aβ(1–42)^{565} aggregates at 37 °C under conditions that permitted CME. Endocytic markers were visualized by immunofluorescence staining (Fig. 9). No colocalization with clathrin (Fig. 9*A*) and LAMP2 (Fig. 9*B*) was observed, supporting that Aβ(1–42) was not internalized via CME. Rather, internalized Aβ(1–42)^{565} colocalized with caveolin (Fig. 9*C*) and EEA1 (Fig. 9*D*), confirming that Aβ(1–42)^{565} was localized in endocytic vesicles and were taken up in a CME-independent pathway.

Discussion

Taken together, our data allow us to map the first steps in Aβ(1–42) internalization starting from the monomeric peptide. First, Aβ(1–42) monomers or very early disordered oligomers bind rapidly to the plasma membrane. Their binding partner could be either the lipid bilayer itself or plasma membrane proteins. Numerous studies have demonstrated interaction of Aβ with lipid bilayers. Its role in Aβ(1–42) uptake will be scrutinized in a future study. There, they aggregate either on the membrane surface itself or in a compartment that is very close to the membrane, from which they are taken up into endocytic vesicles. The highly efficient uptake of β-sheet-rich structures suggests that aggregation into, or co-aggregation with β-sheet aggregates occurs.

For Aβ(1–42) monomers, the peptide concentration has to be sufficient to initiate the first two steps of the process, resulting in a threshold for internalization at the saturation concentration, or critical concentration, for Aβ(1–42) aggregation (22). In contrast, no concentration threshold exists for the internalization of preformed Aβ(1–42) aggregates with β-sheet structure.

This has several implications for the possible mechanism of Aβ(1–42) toxicity. In our experiments metabolic inhibition was directly correlated with the formation and uptake of β-sheet-rich aggregates. Aggregated species have been found to play a central role in Aβ(1–42) toxicity, not all of which are large β-sheet-rich structures (5). Although β-sheet-rich Aβ that was efficiently endocytosed and that inhibited mitochondrial activity could be pelleted at 200,000 × *g* (Fig. 5), very large
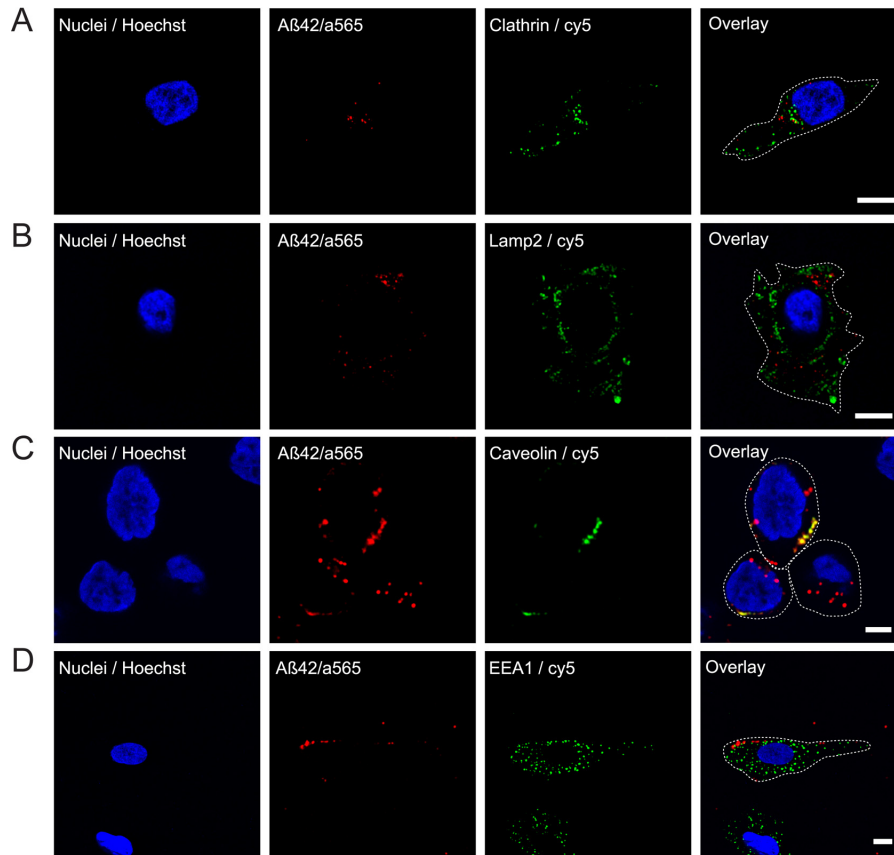
FIGURE 9. **Co-staining of internalized Aβ(1–42) with markers of endocytosis.** SH-EP cells were treated with Aβ(1–42)^{565} aggregates (150 nM, *red*) at 37 °C for 24 h. Colocalization of internalized Aβ(1–42)^{565} detected by clathrin (*A*), LAMP2 (*B*), caveolin (*C*), and EEA1 (*D*) by IF. The primary antibodies of endocytic marker proteins were visualized by Cy5-conjugated secondary antibody (*green*), and were imaged by confocal microscopy. Nuclei were stained with Hoechst 33342 (*blue*). Part of internalized Aβ(1–42)^{565} was colocalized with caveolin and EEA1; but not with clathrin and LAMP2. Cell outlines are marked by *dashed lines* derived from images with increased exposure times (not shown); *scale bars*, 10 μm.

aggregate structures were unable to enter the cell. Our data therefore suggest that neurons preferably take up β-sheet-rich oligomeric and protofibrillar structures of intermediate size. It is tempting to speculate that small oligomers may have a higher affinity to the plasma membrane than the monomeric peptide, facilitating the conversion to β-sheet-rich structures and subsequent internalization. Our results demonstrate that, unlike monomers, preexisting Aβ aggregates are internalized at low nanomolar concentrations, which corresponds to previously observed binding of Aβ oligomers to neuronal plasma membranes at nanomolar concentration (31, 32).

Our experiments did not provide evidence that uptake of aggregates proceeds via CME. Aβ(1–42) can enter the cells via a non-clathrin-mediated pathway, and then locate in the endocytic vesicles. Costaining with caveolin suggests a possible uptake route via the caveolin endocytosis pathway. Aβ(1–42) is also believed to be involved in cholesterol and caveolin trafficking (33).

Aβ(1–42) aggregates may be taken up via receptor independent endocytosis, as had been observed previously (34). Other pathways for the internalization of amyloidogenic proteins have been discussed. Synthetic peptide aggregates of sizes <500 nm were taken up into HEK cells by nonspecific endocytosis, whereas larger aggregates were internalized by a mechanism similar to phagocytosis (35). Tau aggregates can be internalized

via micropinocytosis, mediated by glycosaminoglycans (36). It is possible that Aβ(1–42) aggregates enter the cell by the same pathway.

Second, we found that Aβ(1–42) aggregates can form in a concentration-dependent manner through self-assembly of Aβ(1–42) on the plasma membrane and that internalized Aβ(1–42) aggregates have β-sheet structure. It has long been known that lipid interaction promotes Aβ(1–40) transition to β-sheet structure (37) and our data support the interpretation that this process is central to Aβ uptake and toxicity. Our data suggest the binding of Aβ(1–42) to the lipid bilayer or to membrane proteins may be the first step in the formation of cytotoxic Aβ(1–42) aggregates *de novo*. Factors that increase partitioning of Aβ to the plasma membrane will therefore likely promote the formation of β-sheet-rich aggregates on the membrane. These include lipid peroxidation products, such as seco-cholesterol and 4-hydroxy-nonenal that facilitate Aβ membrane binding and aggregation (38–40), divalent metal ions promoting Aβ membrane interaction (41), and interaction with membrane proteins (16). Our data support a central role of endocytosis in Aβ cytotoxicity (15) and provide strong evidence that aggregation precedes endocytosis, a question that had previously not been conclusively resolved (7, 8). This experimental evidence may improve our understanding of AD pathology and

may inform more focused therapeutic approaches targeting membrane binding and self-assembly of the Aβ peptide.

Experimental Procedures

Preparation of Monomers and Fluorescent Labeling of Aβ(1–42)—Synthetic human Aβ(1–42) and Aβ(1–42) with a single N-terminal cysteine residue (Institute for Medical Immunology, Charité, Berlin, Germany) were dissolved in hexafluoro-2-propanol and incubated at room temperature overnight. After flash freezing by liquid nitrogen, hexafluoro-2-propanol was removed by lyophilization (Savant SpeedVac, Thermo), and the peptides were stored at −20 °C until use.

To prepare unlabeled monomer, lyophilized Aβ(1–42) was dissolved in 10 mM NaOH, sonicated for 30 min in ice-cold water bath, and passed through a 0.22-μm and a 30-kDa filter (Millipore). The monomers were kept on ice and used immediately or within 1 h.

Aβ(1–42) with a single N-terminal cysteine residue was labeled by Atto488-maleimide (Aβ(1–42)[488]), Atto565-maleimide (Aβ(1–42)[565]), or Atto 633-maleimide (Aβ(1–42)[633], Atto Tec) at a 1:1.5 M ratio in NaOH (10 mM) containing 0.05 mM Tris(2-carboxyethyl)phosphine, pH 7.5, and at 4 °C overnight. Aβ(1–42)[565] and free Atto565-maleimide were separated by SEC (Superdex 75, 3.2/20 column, GE Healthcare) with a flow rate at 40 μl/min in 10 mM NaOH.

Scrambled-Aβ(1–42) (Millipore, sc-Aβ(1–42)) was dissolved in 10 mM NaOH and labeled with Atto565-NHS (sc-Aβ(1–42)[565]). The labeling process and the separation of sc-Aβ(1–42)[565] and free dyes were the same as described above. Aβ(1–42) labeled at the N terminus with Hylite555 (Aβ(1–42)[555], Anaspec) was monomerized as described above for unlabeled Aβ(1–42).

Monitoring Aggregation Kinetics of Aβ(1–42) by ThT and SDS-PAGE—Aβ(1–42) monomer aggregation assays were performed in PBS or 50 mM sodium phosphate, pH 7.4, as indicated, containing 20 μM ThT in a microplate reader (InfinitE M200, Tecan, Austria) at 37 °C. ThT fluorescence (excitation wavelength of 440 nm and emission wavelength of 485 nm) was measured every 5 min after 5 s shaking. 50 μl of Aβ(1–42) was removed at different time points as indicated and centrifuged for 30 min at 200,000 $\times$ g (Beckman TL-100). Supernatants were analyzed by denaturing SDS-PAGE.

Circular Dichroism Spectroscopy—Aβ(1–42) samples (15 μM) in PBS were measured in a 1-mm path length cuvette. Circular dichroism (CD) spectra were recorded between 200 and 260 nm with a step size of 1 nm in a CD spectrometer (J-720, Jasco, Japan).

Atomic Force Microscopy—10-μl samples were loaded onto freshly cleaved mica (mica was glued on a glass slide) for 5 min, washed with freshly filtered deionized water (3 $\times$ 100 μl), and dried overnight. All the images were taken using intermittent contact mode on a Nanowizard II/Zeiss Axiovert setup (JPK).

Cell Culture and Cellular Uptake—SH-EP cells were maintained in culture medium (10% (v/v) fetal bovine serum, 4 mM L-glutamine, 110 mg/liter of sodium pyruvate, 100 units/ml of penicillin-streptomycin, 4.5 g/liters of D-glucose in 500 ml of Dulbecco's modified Eagle's medium (Gibco) at 37 °C and 5% CO$_2$. Cells were seeded into 96-well plates or 35-mm cell cul-

ture dishes (MatTek) and grown to about 80% confluence. For cellular uptake, the cells were incubated with Aβ(1–42) or labeled Aβ(1–42) at various concentrations, temperatures, and times. The cells were then washed twice with PBS and fixed with 3.7% paraformaldehyde for 10 min at room temperature. Primary rat hippocampal neurons were a gift of J. Meier, MDC Berlin, and prepared and cultured as previously described (42).

Dot Blot Quantification of Aβ—SH-EP cells were cultured as described above and seeded in a 96-well plate (10,000 cells/well) for quantification of Aβ(1–42) in supernatant and in a 12-well plate (80,000 cells/well) for quantification of Aβ(1–42) in cell lysate. Cells were incubated with monomeric Aβ(1–42) or Aβ(1–42) that was pre-aggregated to the t3 time point (Fig. 5A) in sodium phosphate buffer (50 mM, pH 7.4) as indicated. Cells were washed in PBS, lysed in 100 μl of Tris buffer (50 mM, pH 5.1) containing 2% SDS, and boiled for 10 min. 100 μl of cell lysates or culture media was run through a nitrocellulose membrane (Bio-Rad) on a 96-well vacuum apparatus. Serial dilutions for monomeric and pre-aggregated Aβ(1–42) were spotted in triplicate on the same membrane as the cell samples, and were used as standard reference for calculation of Aβ(1–42) concentrations. The membrane was incubated with blocking buffer (5% BSA in PBS) for 1 h, was washed twice with PBS-T buffer (0.1% Tween 20 in PBS) for 10 min, and then incubated for 1 h with primary antibody, anti-β-amyloid mouse monoclonal antibody (1:500, 6E10, Covance), followed by secondary antibody, IRDyeGAM-800CW (1:15,000, Li-Cor), in PBS-T buffer containing 0.5% BSA. Fluorescence of three replicate wells was evaluated through densitometry. Aβ concentrations were calculated from signals of reference dilution samples by linear regression analysis.

Thioflavin S Staining—Thioflavin S (ThS) was dissolved in 50% ethanol to 1 mg/ml, and stored at 4 °C. Fixed cells were stained with 0.01% ThS for 5 min, washed 3 times with 70% ethanol; incubated with 0.25% KMnO$_4$ for 4 min, rinsed with water; incubated with 1% NaHBO$_4$ for 4 min; then incubated with 3$\times$ PBS (411 mM NaCl, 8.1 mM KCl, 30 mM Na$_2$HPO$_4$, 5.2 mM KH$_2$PO$_4$, pH 7.2) at 4 °C for 30 min and rinsed with water.

For live cell imaging, cells were incubated with ThS at 10 μg/ml in cell culture medium at 37 °C for 10 min. Then the cells were washed five times with PBS and kept in cell culture medium until microscopy.

Immunofluorescence Staining (IF)—To examine if the dye fluorescence of Aβ(1–42)[565] accurately reports the formation of intracellular Aβ(1–42) aggregates and their cellular locations, the cells were co-stained with anti-β-amyloid mouse monoclonal antibody (6E10, Covance), polyclonal anti-amyloid fibril antibody LOC (1:800, Millipore), phalloidin-568 (1:500, Fisher), or endocytic markers by IF after treatment with Aβ(1–42)[565] aggregates. The fixed cells were permeabilized with 0.5% Triton X-100 at room temperature for 5 min, washed twice with PBS. Then cells were incubated with blocking buffer (3% BSA in PBS) at room temperature for 1 h, and were incubated with primary and secondary antibody (diluted at 1:2000) in blocking buffer in the dark at room temperature for 1 h, respectively. The following primary antibodies for endocytic marker proteins were used: anti-caveolin-1 (Santa Cruz), anti-clathrin heavy chain (Abcam), anti-EEA1 (C45B10, Cell Signaling), and anti-

LAMP2 (Abcam) antibodies. Cell nuclei were stained with Hoechst 33342. The dishes were stored in the dark until being viewed by confocal microscopy or epifluorescence microscopy (Zeiss Axiovert, ×63/1.4 NA oil immersion objective) as indicated. Colocalization was analyzed by Pearson correlation analysis using the coloc2 plug-in of Fiji. Thresholded Pearson analysis was used for colocalization of Aβ(1–42)[565] with calcein fluorescence to include only endocytic vesicles that contained calcein.

High-content Screening and Analysis—For HCS experiments, cells were seeded into 96-well plates. The fixed cells were stained with Hoechst 33342 to visualize the nuclei. Nine images per well were recorded by a HCS microscope (Cellomics, Thermo Scientific) with a ×10 objective. For the compartmental analysis, the ArrayScan VTI software was used to identify nuclei by Hoechst 33342 fluorescence, to fit cell dimensions and to identify Aβ(1–42) aggregates through Atto 565 fluorescence (Fig. 4*A*).

MTT Assay—SH-EP cells were seeded into 96-well plates, grown to about 80% confluence and treated with different aggregates species of Aβ(1–42) at various concentrations. Cells were washed to remove extracellular Aβ(1–42). Each experiment was carried out in two separate 96-well plates. One plate was prepared for determination of cell number by HCS microscopy; a parallel plate was used for the MTT assay (Promega). The cells were incubated at 37 °C for 4 h after adding MTT (15 μl/well) and for 1 h after adding solubilization solution (100 μl/well). The absorbance of MTT was recorded at 570 nm using a plate reader. Statistical analysis was performed by Student's t-test assuming two-tailed distributions with equal variances.

Confocal Microscopy and Förster Resonance Energy Transfer (FRET) Image Analysis—All confocal microscopy experiments were performed in 35-mm dishes. The images of fixed samples were recorded with a confocal microscope (Sp5, Leica, Germany, Leica HyD hybrid detector) with an ×63/1.4 NA oil-immersion objective at room temperature. Live cell images were recorded by spinning disc confocal microscopy (Olympus IX83 microscope with Yokogawa CSU-W1 Confocal Spinning Disc unit, Japan, and Evolve 512 EMCCD Camera) with ×60/1.2 NA water immersion objective. Live cell FRET images were recorded with a confocal microscope (Nikon A1Rsi, GaAsP PMT detector) with a ×60/1.4 NA oil immersion objective. For live cell images, the temperature of the incubation chamber on the microscope was set to 37 °C, and 5% CO_2 was filled into the incubation chamber. The fluorescence was measured for Hoechst 33342 with excitation wavelength of 405 nm and emission wavelengths of 420–460 nm; Atto488 with excitation wavelength of 488 nm and emission wavelengths of 500–600 nm; Atto565 with excitation wavelengths of 543, 561, or 565 nm and emission wavelengths of 550 or 580–610 nm; Atto633 and Cy5 with excitation wavelengths of 633 or 640 nm and emission wavelengths of 650–800 nm; calcein with excitation wavelength of 488 nm and emission wavelengths of 490–540 nm.

The images for sensitized emission FRET analysis were recorded by confocal microscopy described as above. For Atto488-Atto633 FRET pair, the fluorescence was measured with excitation wavelengths of 488, 633, and 488 and emission wavelengths of 500–600, 650–800, and 650–800 nm for Atto488, Atto633, and Aβ(1–42)[488] to Aβ(1–42)[633] FRET, respectively. Correspondingly, FRET between Hylite 555 and Atto633 was calculated from confocal images recorded with excitation at 561, 638, and 561 nm and emission at 570–600, 650–800, and 650–800 nm. Corrected FRET images were calculated from FRET, donor, and acceptor pixel intensities using the Fiji distribution and the PixFRET plug-in (43). The corrected FRET intensity for each pixel is given by,

$$I_{FRET} = I^0_{FRET} - BT_{donor} \times I_{donor} - BT_{acceptor} \times I_{acceptor}$$

(Eq. 1)

where I_{FRET} is the raw fluorescence intensity of the FRET channel, I_{donor} and $I_{acceptor}$ are the fluorescence intensities of the donor (Atto488 or Hylite 555) and acceptor (Atto633), respectively. I_{FRET} is normalized (nFRET) as a function of the square root of the product of donor and acceptor intensities.

$$nFRET = \frac{I_{FRET}}{\sqrt{I_{donor} \times I_{acceptor}}} \times 100$$

(Eq. 2)

Intensity-independent donor and acceptor bleed-through (BT) were determined by,

$$BT_{donor} = \frac{I_{FRET}}{I_{donor}}$$

(Eq. 3)

$$BT_{acceptor} = \frac{I_{FRET}}{I_{acceptor}}$$

(Eq. 4)

which were fitted with a linear model.

In vitro FRET of Aβ(1–42)[488]/Aβ(1–42)[633] was calculated as the ratio of $I_{acceptor}$ (645 nm)/I_{donor} (530 nm) after excitation at 488 nm in a Spectramax i3x (Molecular Devices) fluorescence plate reader.

References

1. Glenner, G. G., and Wong, C. W. (1984) Alzheimer's disease: initial report of the purification and characterization of a novel cerebrovascular amyloid protein. *Biochem. Biophys. Res. Commun.* **120,** 885–890

2. Simons, M., Keller, P., De Strooper, B., Beyreuther, K., Dotti, C. G., and Simons, K. (1998) Cholesterol depletion inhibits the generation of β-amyloid in hippocampal neurons. *Proc. Natl. Acad. Sci. U.S.A.* **95,** 6460–6464

3. Shoji, M., Golde, T. E., Ghiso, J., Cheung, T. T., Estus, S., Shaffer, L. M., Cai, X. D., McKay, D. M., Tintner, R., and Frangione, B. (1992) Production of the Alzheimer amyloid β protein by normal proteolytic processing. *Science* **258,** 126–129

4. Jarrett, J. T., Berger, E. P., and Lansbury, P. T. (1993) The carboxy terminus of the β amyloid protein is critical for the seeding of amyloid formation: implications for the pathogenesis of Alzheimer's disease. *Biochemistry.* **32,** 4693–4697

5. Walsh, D. M., Klyubin, I., Fadeeva, J. V., Cullen, W. K., Anwyl, R., Wolfe, M. S., Rowan, M. J., and Selkoe, D. J. (2002) Naturally secreted oligomers of amyloid β protein potently inhibit hippocampal long-term potentiation *in vivo. Nature* **416,** 535–539

6. Ida, N., Masters, C. L., and Beyreuther, K. (1996) Rapid cellular uptake of Alzheimer amyloid βA4 peptide by cultured human neuroblastoma cells. *FEBS Lett.* **394,** 174–178

7. Hu, X., Crick, S. L., Bu, G., Frieden, C., Pappu, R. V., and Lee, J-M. (2009) Amyloid seeds formed by cellular uptake, concentration, and aggregation of the amyloid-β peptide. *Proc. Natl. Acad. Sci. U.S.A.* **106,** 20324–20329

8. Friedrich, R. P., Tepper, K., Rönicke, R., Soom, M., Westermann, M., Reymann, K., Kaether, C., and Fändrich, M. (2010) Mechanism of amyloid plaque formation suggests an intracellular basis of Aβ pathogenicity. *Proc. Natl. Acad. Sci. U.S.A.* **107,** 1942–1947

9. Frost, B., Ollesch, J., Wille, H., and Diamond, M. I. (2009) Conformational diversity of wild-type Tau fibrils specified by templated conformation change. *J. Biol. Chem.* **284,** 3546–3551

10. Brundin, P., Melki, R., and Kopito, R. (2010) Prion-like transmission of protein aggregates in neurodegenerative diseases. *Nat. Rev. Mol. Cell Biol.* **11,** 301–307

11. Sanders, D. W., Kaufman, S. K., DeVos, S. L., Sharma, A. M., Mirbaha, H., Li, A., Barker, S. J., Foley, A. C., Thorpe, J. R., Serpell, L. C., Miller, T. M., Grinberg, L. T., Seeley, W. W., and Diamond, M. I. (2014) Distinct Tau prion strains propagate in cells and mice and define different tauopathies. *Neuron* **82,** 1271–1288

12. Prusiner, S. B. (1998) Prions. *Proc. Natl. Acad. Sci. U.S.A.* **95,** 13363–13383

13. Bieschke, J., Weber, P., Sarafoff, N., Beekes, M., Giese, A., and Kretzschmar, H. (2004) Autocatalytic self-propagation of misfolded prion protein. *Proc. Natl. Acad. Sci. U.S.A.* **101,** 12207–12211

14. Frost, B., and Diamond, M. I. (2010) Prion-like mechanisms in neurodegenerative diseases. *Nat. Rev. Neurosci.* **11,** 155–159

15. Yu, A., Shibata, Y., Shah, B., Calamini, B., Lo, D. C., and Morimoto, R. I. (2014) Protein aggregation can inhibit clathrin-mediated endocytosis by chaperone competition. *Proc. Natl. Acad. Sci. U.S.A.* **111,** E1481–E1490

16. Lai, A. Y., and McLaurin, J. (2010) Mechanisms of amyloid-β peptide uptake by neurons: the role of lipid rafts and lipid raft-associated proteins. *Int. J. Alzheimers. Dis.* **2011,** 548380

17. Holmes, B. B., DeVos, S. L., Kfoury, N., Li, M., Jacks, R., Yanamandra, K., Ouidja, M. O., Brodsky, F. M., Marasa, J., Bagchi, D. P., Kotzbauer, P. T., Miller, T. M., Papy-Garcia, D., and Diamond, M. I. (2013) Heparan sulfate proteoglycans mediate internalization and propagation of specific proteopathic seeds. *Proc. Natl. Acad. Sci. U.S.A.* **110,** E3138–E3147

18. Treusch, S., Hamamichi, S., Goodman, J. L., Matlack, K. E., Chung, C. Y., Baru, V., Shulman, J. M., Parrado, A., Bevis, B. J., Valastyan, J. S., Han, H., Lindhagen-Persson, M., Reiman, E. M., Evans, D. A., Bennett, D. A., *et al.* (2011) Functional links between A toxicity, endocytic trafficking, and Alzheimer's disease risk factors in yeast. *Science* **334,** 1241–1245

19. Kanekiyo, T., Cirrito, J. R., Liu, C-C., Shinohara, M., Li, J., Schuler, D. R., Shinohara, M., Holtzman, D. M., and Bu, G. (2013) Neuronal

20. clearance of amyloid-β by endocytic receptor LRP1. *J. Neurosci.* **33,** 19276–19283

20. LeVine, H., 3rd. (1993) Thioflavine T interaction with synthetic Alzheimer's disease β-amyloid peptides: detection of amyloid aggregation in solution. *Protein Sci.* **2,** 404–410

21. LeVine, H., 3rd. (1999) Quantification of β-sheet amyloid fibril structures with thioflavin T. *Methods Enzymol.* **309,** 274–284

22. Usui, K., Hulleman, J. D., Paulsson, J. F., Siegel, S. J., Powers, E. T., and Kelly, J. W. (2009) Site-specific modification of Alzheimer's peptides by cholesterol oxidation products enhances aggregation energetics and neurotoxicity. *Proc. Natl. Acad. Sci. U.S.A.* **106,** 18563–18568

23. Bieschke, J., Russ, J., Friedrich, R. P., Ehrnhoefer, D. E., Wobst, H., Neugebauer, K., and Wanker, E. E. (2010) EGCG remodels mature α-synuclein and amyloid-β fibrils and reduces cellular toxicity. *Proc. Natl. Acad. Sci. U.S.A.* **107,** 7710–7715

24. Wei, J., Wu, C., Lankin, D., Gulrati, A., Valyi-Nagy, T., Cochran, E., Pike, V. W., Kozikowski, A., and Wang, Y. (2005) Development of novel amyloid imaging agents based upon thioflavin S. *Curr. Alzheimer Res.* **2,** 109–114

25. Harding, C., Heuser, J., and Stahl, P. (1983) Receptor-mediated endocytosis of transferrin and recycling of the transferrin receptor in rat reticulocytes. *J. Cell Biol.* **97,** 329–339

26. Iacopetta, B. J., Morgan, E. H., and Yeoh, G. C. (1983) Receptor-mediated endocytosis of transferrin by developing erythroid cells from the fetal rat liver. *J. Histochem. Cytochem.* **31,** 336–344

27. Jandl, J. H., and Katz, J. H. (1963) The plasma-to-cell cycle of transferrin. *J. Clin. Invest.* **42,** 314–326

28. Laurell, C., and Ingelman, B. (1947) The iron-binding protein of swine serum. *Acta Chem. Scand.* **1,** 770–776

29. Uzman, A., Lodish, H., Berk, A., Zipursky, L., and Baltimore, D. (2000) Molecular Cell Biology. *Biochem. Mol. Biol. Educ.* **29,** Section 5.3

30. Lodish, H. F., Berk, A., Zipursky, S. L., Matsudaira, P., Baltimore, D., and James, D. (2008) *Molecular Cell Biology*, 10.1016/S1470-8175(01)00023-6, W. H. Freeman, San Franscisco, CA

31. Johnson, R. D., Schauerte, J. A., Chang, C. C., Wisser, K. C., Althaus, J. C., Carruthers, C. J., Sutton, M. A., Steel, D. G., and Gafni, A. (2013) Single-molecule imaging reveals Aβ42:Aβ40 ratio-dependent oligomer growth on neuronal processes. *Biophys. J.* **104,** 894–903

32. Johnson, R. D., Schauerte, J. A., Wisser, K. C., Gafni, A., and Steel, D. G. (2011) Direct observation of single amyloid-β(1– 40) oligomers on live cells: binding and growth at physiological concentrations. *PLoS ONE* **6,** e23970

33. Igbavboa, U., Sun, G. Y., Weisman, G. A., He, Y., and Wood, W. G. (2009) Amyloid β-protein stimulates trafficking of cholesterol and caveolin-1 from the plasma membrane to the Golgi complex in mouse primary astrocytes. *Neuroscience* **162,** 328–338

34. Omtri, R. S., Davidson, M. W., Arumugam, B., Poduslo, J. F., and Kandimalla, K. K. (2012) Differences in the cellular uptake and intracellular itineraries of amyloid β proteins 40 and 42: ramifications for the Alzheimer's drug discovery. *Mol. Pharm.* **9,** 1887–1897

35. Couceiro, J. R., Gallardo, R., De Smet, F., De Baets, G., Baatsen, P., Annaert, W., Roose, K., Saelens, X., Schymkowitz, J., and Rousseau, F. (2015) Sequence-dependent internalization of aggregating peptides. *J. Biol. Chem.* **290,** 242–258

36. Holmes, B. B., Furman, J. L., Mahan, T. E., Yamasaki, T. R., Mirbaha, H., Eades, W. C., Belaygorod, L., Cairns, N. J., Holtzman, D. M., and Diamond, M. I. (2014) Proteopathic tau seeding predicts tauopathy *in vivo. Proc. Natl. Acad. Sci. U.S.A.* **111,** E4376–E4385

37. Terzi, E., Hölzemann, G., and Seelig, J. (1995) Self-association of β-amyloid peptide (1– 40) in solution and binding to lipid membranes. *J. Mol. Biol.* **252,** 633–642

38. Bieschke, J., Zhang, Q., Powers, E. T., Lerner, R. A., and Kelly, J. W. (2005) Oxidative metabolites accelerate Alzheimer's amyloidogenesis by a two-step mechanism, eliminating the requirement for nucleation. *Biochemistry* **44,** 4977–4983

39. Siegel, S. J., Bieschke, J., Powers, E. T., and Kelly, J. W. (2007) The oxidative stress metabolite 4-hydroxynonenal promotes Alzheimer protofibril formation. *Biochemistry* **46,** 1503–1510

40. Murray, I. V., Liu, L., Komatsu, H., Uryu, K., Xiao, G., Lawson, J. A., and Axelsen, P. H. (2007) Membrane-mediated amyloidogenesis and the promotion of oxidative lipid damage by amyloid β proteins. *J. Biol. Chem.* **282,** 9335–9345

41. Curtain, C. C., Ali, F. E., Smith, D. G., Bush, A. I., Masters, C. L., and Barnham, K. J. (2003) Metal ions, pH, and cholesterol regulate the interactions of Alzheimer's disease amyloid-β peptide with membrane lipid. *J. Biol. Chem.* **278,** 2977–2982

42. Winkelmann, A., You, X., Grünewald, N., Häussler, U., Krestel, H., Haas, C. A., Schwarz, G., Chen, W., and Meier, J. C. (2015) Identification of a new genomic hot spot of evolutionary diversification of protein function. *PLoS ONE* **10,** e0125413

43. Feige, J. N., Sage, D., Wahli, W., Desvergne, B., and Gelman, L. (2005) PixFRET, an ImageJ plug-in for FRET calculation that can accommodate variations in spectral bleed-through. *Microsc. Res. Tech.* **68,** 51–58

Supplementary data

Amyloid–β 1–42 aggregation initiates its cellular uptake and cytotoxicity

Sha Jin[1, 2], Niraja Kedia[2],Eva Illes–Toth[2], Ivan Haralampiev[3], Simon Prisner[3], Andreas Herrmann[4], Erich E. Wanker[1] and Jan Bieschke[2]

[1]Proteomics and Molecular Mechanisms of Neurodegenerative Diseases, Max Delbrück Center for Molecular Medicine, Berlin–Buch, Germany

[2]Department of Biomedical Engineering, Washington University in St. Louis, MO, USA

[3] Department of Biology, Humboldt–Universität zu Berlin, Berlin, Germany

[4]Department of Biology, IRI Life Sciences, Humboldt–Universität zu Berlin, Berlin, Germany

Supplementary Figure 1: Live cell FRET imaging of Aβ internalization. SHEP cells were incubated with fibrillar $A\beta_{1-42}^{633}$ (150 nM) for 30 min followed by monomeric $A\beta_{1-42}^{555}$ (150 nM). Co-aggregation of monomeric and fibrillar $A\beta_{1-42}$ was quantified by FRET analysis. Beta-sheet structures were co-stained with ThS. Shown is one representative time course out of four independent experiments.

Supplementary Figure 1
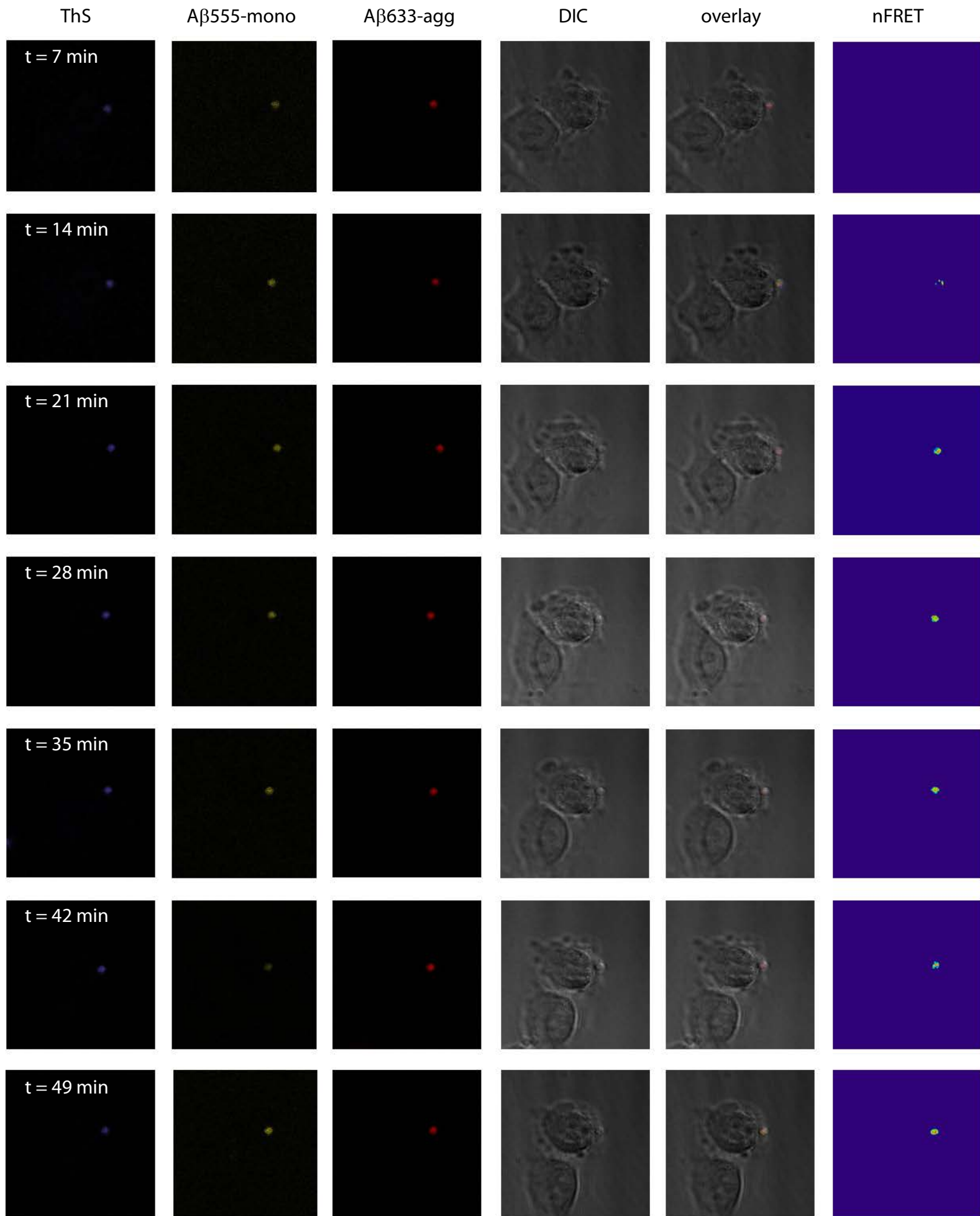
Amyloid-β(1−42) Aggregation Initiates Its Cellular Uptake and Cytotoxicity

Sha Jin, Niraja Kedia, Eva Illes-Toth, Ivan Haralampiev, Simon Prisner, Andreas Herrmann, Erich E. Wanker and Jan Bieschke